ALKBH5 regulates somatic cell reprogramming in a phase specific manner

Sherif Khodeer[1, 3*], Arne Klungland[1, 2], John Arne Dahl[1*]

[1] Department of Microbiology, Oslo University Hospital, Rikshospitalet, Forskningsveien 1, 0373. Oslo, Norway.

[2] Department of Biosciences, Faculty of Mathematics and Natural Sciences, University of Oslo, 0316. Oslo, Norway.

[3] Current affiliation: KU Leuven-University of Leuven, Department of Development and Regeneration, Leuven Institute for Single-cell Omics (LISCO), Leuven Stem Cell Institute, Leuven, Belgium.

[*]Correspondence

Sherif Khodeer and John Arne Dahl

Department of Microbiology, Oslo University Hospital, Rikshospitalet, Forskningsveien 1, 0373. Oslo, Norway.

KU Leuven-University of Leuven, Department of Development and Regeneration, Leuven Institute for Single-cell Omics (LISCO), Leuven Stem Cell Institute, Leuven, Belgium.

Emails: Sherif.Khodeer@Kkuleuven.be , j.a.dahl@medisin.uio.no

Keywords: *Alkbh5*, reprogramming, induced pluripotent stem cells (iPSCs), *Nanog*.

Summary statement: ALKBH5 in somatic cell reprogramming

Abstract

Establishment of the pluripotency regulatory network in somatic cells by introducing four transcription factors (octamer binding transcription factor 4 (OCT4), sex determining region Y (SRY)-box 2 (SOX2), Kruppel-like factor 4 (KLF4), and cellular myelocytomatosis (c-MYC)) provides a promising tool for cell-based therapies in regenerative medicine. Nevertheless, the mechanisms at play when generating induced pluripotent stem cells from somatic cells are only partly understood. Here, we show that the RNA specific N6-methyladenosine (m^6A) demethylase ALKBH5 regulates somatic cell reprogramming in a stage-specific manner through its catalytic activity. Knockdown or knockout of *Alkbh5* in the early reprogramming phase impairs reprogramming efficiency by reducing the proliferation rate through arresting the cells at G2/M phase and decreasing the upregulation of epithelial markers. On the other hand, ALKBH5 overexpression at the early reprogramming phase has no significant impact on reprogramming efficiency, while overexpression at the late phase enhances reprogramming by stabilizing *Nanog* transcripts, resulting in upregulated *Nanog* expression. Our study provides mechanistic insight into the crucial dynamic role of ALKBH5 through its catalytic activity in regulating somatic cell reprogramming at the posttranscriptional level.

Introduction

The four transcription factors OCT4, SOX2, KLF4, and c-MYC (OSKM) are sufficient to reprogram and induce pluripotency when ectopically expressed in mouse or human somatic cells to generate induced pluripotent stem cells (iPSCs) (Takahashi et al., 2007, Takahashi and Yamanaka, 2006). These reprogrammed iPSCs are highly similar to their pluripotent embryonic stem cell (ESC) counterparts in transcriptional profile and epigenetic

landscape (Chin et al., 2009, Deng et al., 2009, Guenther et al., 2010) and show infinite self-renewal capability (Takahashi and Yamanaka, 2006) and the ability to differentiate into the three germ layers *in vivo* and *in vitro* (Carey et al., 2011). Therefore, iPSC technology provides an ideal tool for drug screening and patient-specific disease modeling, and holds great promise for therapeutic applications in the future (Onder and Daley, 2012).

The early phase of the reprogramming process is characterized by stochastic events (Buganim et al., 2012), in which mesenchymal genes are downregulated, while epithelial genes are upregulated in a process known as mesenchymal-epithelial transition (MET), together with clear morphological transformation accompanied by an increased proliferation rate to form cell clusters (Samavarchi-Tehrani et al., 2010, Li et al., 2010). However, most fibroblasts exposed to iPSC reprogramming conditions fail to achieve proper morphological changes and remain in a fibroblast like morphology. These trapped cells undergo senescence, apoptosis, and cell cycle arrest, which in turn explain the low efficiency of the reprogramming process (Stadtfeld and Hochedlinger, 2010, Banito et al., 2009, Kim et al., 2018). In addition, several studies have demonstrated that cell cycle regulators, including p21, p53 and p16/INK4A, are barriers to the reprogramming process and that their depletion enhances the reprogramming process (Kawamura et al., 2009, Li et al., 2009, Hong et al., 2009, Utikal et al., 2009).

The late phase of the reprogramming process is considered deterministic, in which reactivation of endogenous *Sox2* expression is considered a rate-limiting step for acquiring ESC identity (Buganim et al., 2012). This phase is also characterized by removal of somatic epigenetic memory, telomere elongation, expression of endogenous pluripotency genes, and establishment of pluripotency specific epigenetic and transcriptional profiles (Li et al., 2010, Samavarchi-Tehrani et al., 2010).

The N6-methyladenosine (m^6A) modification, methylation of the N6 position of the adenosine base, is the most abundant internal posttranscriptional modification in mammalian mRNA (Zhang et al., 2019). It was recently shown that m^6A modification is reversible and that its presence is regulated through coordination of several modulators (Jia et al., 2011, Zheng et al., 2013). The positioning of m^6A is mediated by methyl transferase-like 3 (METLL3), methyl transferase-like 14 (METLL14) and Wilms′ tumor 1-associating protein (WTAP) (Bokar et al., 1997, Schwartz et al., 2014, Liu et al., 2014, Ping et al., 2014). Removal of m^6A is carried out by the demethylases fat mass and obesity-associated protein (FTO) and alkylated DNA repair protein AlkB homolog 5 (ALKBH5) (Gerken et al., 2007, Zheng et al., 2013). Furthermore, the m^6A modification is recognized and bound by readers, including YTH domain-containing proteins 1-3 (YTHDF1-3) and YTHDC1 and 2, which in turn facilitate downstream processing, such as mRNA splicing, stabilization, translation or degradation (Dominissini et al., 2012, Wang et al., 2014, Alarcón et al., 2015).

ALKBH5 is one of nine mammalian members of the AlkB family of Fe(II)- and α-ketoglutarate-dependent dioxygenases and can demethylate the m^6A modification in RNA to adenosine (A) (Zheng et al., 2013). We have previously shown that *Alkbh5* is highly expressed in meiotic cells of the testis and is mainly localized to the nucleus (Zheng et al., 2013). ALKBH5 has been shown to regulate various biological and pathophysiological processes including: meiosis, gametogenesis, autophagy, glioblastoma, breast cancer, lung cancer and infertility (Tang et al., 2018, Zheng et al., 2013, Song et al., 2019, Chao et al., 2020, Zhang et al., 2016, Zhang et al., 2017). In addition, the heterogeneity in *Alkbh5* expression in several cancer models has led to suggestions of a putative oncogenic or tumor suppressive role (Wang et al., 2020). Despite extensive studies on ALKBH5 in different biological systems, the functional and regulatory role of ALKBH5 in somatic cell reprogramming has not been addressed. In this study, we dissected the precise role of

ALKBH5 in the reprogramming process, and our data revealed that ALKBH5 plays a biphasic role during somatic cell reprogramming. Depletion of *Alkbh5* in the very early phase of reprogramming impairs the reprogramming process through downregulation of Cyclin B1 and B2, resulting in a reduction in the cell proliferation rate and arresting cells at G2/M phase accompanied by a decrease in the rate of MET. In the late phase, overexpression of ALKBH5 stabilizes *Nanog* transcripts, resulting in upregulated *Nanog* expression, which in turn enhances the reprogramming efficiency.

Results

ALKBH5 depletion in the early phase impairs reprogramming efficiency

To explore the role of ALKBH5 in reprogramming, we first examined the expression of *Alkbh5* during the reprogramming process, and we found that the expression of ALKBH5 was gradually upregulated during reprogramming at both the mRNA and protein levels (Fig. 1A, B). Then, we used two different short hairpin RNAs (shRNAs) to knockdown *Alkbh5* expression (Fig. 1C). As expected by knocking down *Alkbh5*, we found that the total m^6A level at mRNA was highly increased compared to the controls (supplementary Fig. 1A)

Next, we established a reprogramming system in which *Alkbh5* was knocked down 2 days before induction of retroviral reprogramming factors (OSKM) in mouse embryonic fibroblasts (MEFs). We used Δ-PE-Oct4-GFP transgenic reporter MEFs (OG2 MEFs) in which GFP expression is encoded by the distal enhancer regulatory region of Oct4 as a stringent marker for establishment of a naiive pluripotency network (Rais et al., 2013, Mor et al., 2018, Velychko et al., 2019). Then, we assessed the reprogramming efficiency by counting the number of GFP positive colonies and by flow cytometry of the GFP positive

fraction on day 14 (Fig. 1D). Interestingly, *Alkbh5* knockdown significantly reduced the reprogramming efficiency by decreasing both the percentage of the Δ-PE-Oct4-GFP positive fraction and the number of GFP positive colonies on day 14 (Fig. 1E, F). Furthermore, we established another reprogramming system using nontransgenic MEFs and assessed the reprogramming efficiency by measuring the percentage of stage-specific embryonic antigen 1 (SSEA1) positive cells (an early reprogramming marker) on day 7 and the number of ALP positive colonies on day 14 (supplementary Fig. 1B). In agreement with our previous data, *Alkbh5* knockdown significantly reduced the reprogramming efficiency by decreasing the percentage of SSEA1 positive cells on day 7 and the number of ALP positive colonies on day 14 compared to controls (Fig. 1G, H). In addition, we used flow cytometry to assess the percentage of the Δ-PE-Oct4-GFP positive population gated on the SSEA1 positive fraction. Our data revealed that knockdown of *Alkbh5* reduced the percentage of the Δ-PE-Oct4-GFP positive population compared to the control (supplementary Fig. 1C). To substantiate these data, we derived *Alkbh5* knockout (KO) MEFs and found that the reprogramming efficiency of *Alkbh5* (KO) MEFs was greatly reduced compared to that of wild-type (WT) MEFs on either day 7 or day 14 as revealed by the decreased percentage of SSEA1 positive cells (Fig. 1I and supplementary Fig. 1D, E) (Zheng et al., 2013). Taken together, these data suggest that *Alkbh5* depletion at the early phase of reprogramming impairs somatic cell reprogramming.

To further characterize the time-specific role of ALKBH5, we took advantage of a doxycycline (Dox)-inducible short hairpin RNA (shRNA) expression system to suppress the expression of *Alkbh5* at specific time points during reprogramming (Supplementary Fig. 1F). We found that *Alkbh5* knockdown at the very early stage of reprogramming, earlier than day 3, had the largest impact on reducing the reprogramming efficiency, as shown by the decreased fraction of SSEA1 positive cells on days 7 and 14 of reprogramming (Supplementary Fig. 1G). On the other hand, we did not see any significant change in

reprogramming efficiency when *Alkbh5* was knocked down specifically at a later time than day 3 of the reprogramming process (Supplementary Fig. 1G, H). To confirm our data, we used Δ-PE-Oct4-GFP reporter MEFs coupled with a Dox-inducible *Alkbh5* knockdown system and treated the cells with Dox for two days, for seven different time intervals (day 0-2; 2-4; 4-6; 6-8; 8-10; 10-12 and 12-14) throughout the whole reprogramming process until day 14. Then, we assessed the reprogramming efficiency on day 14 using flow cytometry. Consistent with our previous results, we found that only knockdown of *Alkbh5* in the very early stage, day 0-2 and day 2-4, impaired the reprogramming efficiency (Fig. 1G,H and Supplementary Fig. 1I).

Furthermore, we derived homozygous floxed *Alkbh5* (*Alkbh5* $^{f/f}$) MEFs, and we used a 4-hydroxy tamoxifen (4-OH Tam)-inducible Cre recombinase system in which Cre was flanked by mutated ligand-binding domains of the murine estrogen receptor (Mer-Cre-Mer) to deplete *Alkbh5* at specific time points during reprogramming (Supplementary Fig. 1J-L) (Zheng et al., 2013). Consistent with our time-specific knockdown data, depletion of *Alkbh5* only at the very early stage (day 2) of reprogramming impairs reprogramming, as measured by a decreased percentage of SSEA1-positive cells in the population (Fig. 1J). Time-specific depletion of *Alkbh5* at day 8 or 10 of reprogramming had no significant impact on the reprogramming efficiency (Supplementary Fig. 1M). We further confirmed our data by treating homozygous floxed *Alkbh5* MEFs with (4-OH Tam) to deplete *Alkbh5* at different time points of reprogramming, and we found that only *Alkbh5* depletion on day 2 or day 4 had a major impact on reducing the reprogramming efficiency, as measured by alkaline phosphate staining at day 14 (Supplementary Fig. 1N). In conclusion, only *Alkbh5* depletion at the very early stage of reprogramming negatively affects the reprogramming process.

ALKBH5 regulates reprogramming through its m6A demethylase activity

Next, we asked whether the regulatory effect of ALKBH5 on somatic reprogramming is due to its m6A demethylase activity. We constructed two different mutants of ALKBH5 tagged with a carboxyl terminal hemagglutinin (HA) tag. The first one has a point mutation in the catalytic domain in which histidine (H) at position 205 is replaced with alanine (A) to create catalytically inactive mouse ALKBH5 (H205A) (Zheng et al., 2013). In the second one, we completely deleted the catalytic domain to create catalytically dead ALKBH5 (CD) (Fig. 2A and supplementary Fig. 2A). Then, we overexpressed either WT ALKBH5-HA, ALKBH5 (H205A), or ALKBH5 (CD) in both WT and KO *Alkbh5* MEFs, and we confirmed the overexpression by immunoblotting (Fig. 2B, and supplementary Fig. 2B). Next, we assessed the effect of overexpression on reprogramming using Δ-PE-Oct4-GFP by counting the number of GFP positive colonies and by flow cytometry on day 14. We found that overexpression of WT ALKBH5-HA enhances the reprogramming process as assessed on day 14, and it was able to rescue the reduction in reprogramming efficiency elicited by shRNA construct number 2, which targets the 3` untranslated region (3`UTR) of *Alkbh5* (Supplementary Fig. 2C). Interestingly, overexpression of either ALKBH5-HA (H205A) or ALKBH5-HA (CD) was not able to rescue the knockdown of *Alkbh5*, but decreased the reprogramming efficiency in WT MEFs (Fig. 2C, D). To further validate our data, we overexpressed either WT ALKBH5-HA, ALKBH5-HA (H205), or ALKBH5 (CD) on day 1 of reprogramming in both WT and KO *Alkbh5* MEFs. Our data revealed that overexpression of ALKBH5-HA enhanced reprogramming efficiency by increasing the number of ALP positive colonies in both WT and KO *Alkbh5* MEFs (Fig. 2E, F). However, overexpression of ALKBH5-HA (H205A) or ALKBH5-HA (CD) decreased the number of ALP positive colonies in WT MEFs and was not able to increase the number of ALP positive colonies in KO *Alkbh5* MEFs (Fig. 2E, F). In addition, our analysis of the SSEA1 positive fraction on day

7 and day 14 by flow cytometry revealed that overexpression of WT ALKBH5-HA in the early phase of reprogramming until day 7 did not have any impact on reprogramming efficiency. However, overexpression of WT ALKBH5-HA in the late stage of reprogramming, after day 7, increased reprogramming efficiency. In addition, overexpression of ALKBH5-HA (H205A) or ALKBH5-HA (CD) in WT or KO *Alkbh5* MEFs reduced the reprogramming efficiency as assessed by a decrease in the fraction of the SSEA1 positive cells (Supplementary Fig. 2D). It is worth mentioning that *Alkbh5* KO MEFs exhibited a reduced proliferation rate compared to WT MEFs, and overexpression of WT ALKBH5-HA in *Alkbh5* KO MEFs restored the proliferation rate. Overexpression of either ALKBH5-HA (H205A) or ALKBH5-HA (CD) was unable to restore the proliferation rate in *Alkbh5* KO MEFs, and surprisingly decreased the proliferation rate in *Alkbh5* WT MEFs (Supplementary Fig. 2E). Taken together, our data revealed that ALKBH5 regulates somatic cell reprogramming through its m6A demethylase activity. Overexpression of either the ALKBH5-HA (H205A) or ALKBH5-HA (CD) had a negative effect on the reprogramming process and was not able to rescue the phenotype of *Alkbh5* KO MEFs.

Effect of *Alkbh5* removal during the early phase of reprogramming on cell cycle regulators and MET

To investigate the mechanism involved in reduced reprogramming efficiency resulting from loss of *Alkbh5*, we focused on two important events: cell proliferation and MET, which have both been reported to be critical to the early phase of reprogramming (Li et al., 2010, Samavarchi-Tehrani et al., 2010). First, we explored the impact of *Alkbh5* removal on proliferation and apoptosis during the early phase of reprogramming. Our data revealed that *Alkbh5* knockdown during the early phase of reprogramming increased the percentage of cells

at G2/M phase (Fig. 3A, B). Additionally, *Alkbh5* depletion resulted in reduced cell proliferation during reprogramming, which is consistent with our data on *Alkbh5* KO MEFs (Fig. 3C and Supplementary Fig. 2E). However, we did not observe any significant changes in the percentage of Annexin positive cells as compared to the control, indicating that the reduction in cell number is mainly due to G2/M cell cycle arrest and not due to cell apoptosis (Supplementary Fig. 3A-C). Overexpression of ALKBH5-HA during reprogramming did not have any impact on the cell cycle phases or cell proliferation rate (supplementary Fig. 3D-F). Next, we assessed the expression of factors of the mitotic checkpoint complex (MCC) and found that Cyclin B1 and B2 were markedly downregulated at both the RNA and protein levels after knocking down ALKBH5 during the early phase of reprogramming (Fig. 3D, E). Other MCC factors, such as *Cdc20*, *Mad1*, *Mad2*, *Bub1* and *Bub3*, or G1 phase cell cycle regulators, such as *p16* and *p19*, were not significantly affected (Fig. 3D, E and supplementary Fig. 3G). To validate our *Alkbh5* knockdown data, we used *Alkbh5*$^{f/f}$ MEFs and induced *Alkbh5* removal by 4-OH Tam 8 hours after reprogramming induction. In agreement with our knockdown data, we found a reduction in Cyclin B1 and B2 levels, showing that this phenotype presents with the loss of *Alkbh5* both in MEFs and in the early reprogramming process (Supplementary Fig. 3H). It is also noteworthy that depletion of *Alkbh5* in MEFs decreased the proliferation rate and induced cell cycle arrest at G2/M phase accompanied by a reduction in the protein levels of both Cyclin B1 and B2 (Supplementary Fig. 3I- L). This is consistent with what we observed during reprogramming (Fig. 3A –E and supplementary Fig. 2E). The phenotype of *Alkbh5* KO MEFs urged us to eliminate the possibility that nonretroviral infected MEFs have an impact on the readout of reprogramming efficiency. We assessed the infection efficiency using retroviral pMXs-DsRed as a control. Our infection efficiency was higher than 90%, as estimated by flow cytometry (Supplementary Fig. 3 M-O) (Okita et al., 2010). Then, we assessed the reprogramming efficiency using double gating of

both DsRed and SSEA1 on day 7 and day 14 in WT and KO *Alkbh5* MEFs with or without ALKBH5-HA overexpression. Our data revealed that the SSEA1 positive population emerges from the DsRed positive population, and the percentage of SSEA1 positive cells is decreased in KO *Alkbh5* MEFs on both day 7 and day 14, but increased on day 14 in the case of ALKBH5-HA overexpression compared to WT MEFs (Supplementary Fig. 3P). To further support these data, we applied the piggyBac (PB) transposon reprogramming system in which the polycistronic reprogramming cassette (OSKM) is under the tetracycline regulatory (Tet-ON) promoter and separated from the m-Cherry fluorescent protein by an internal ribosome entry site (IRES) for simultaneous tracking of the reprogrammed population (Supplementary Fig. 3O, Q) (Kim et al., 2015). Our data obtained with the PB transposon reprogramming system were very similar to the retroviral reprogramming results, which not only substantiated our findings but also indicated that the regulatory role of ALKBH5 in reprogramming is relevant to both reprogramming methodologies (Supplementary Fig. 3R). Thereafter, we assessed the MET process at day 6 of reprogramming in which *Alkbh5* was knocked down 2 days before reprogramming induction (Supplementary Fig. 3S). Our qPCR and western blot data revealed that *Alkbh5* depletion impairs the MET process by decreasing the rate of downregulation of mesenchymal markers such as platelet-derived growth factor receptor beta (*PDGFRβ*), Snail family zinc finger 2 (*Slug*), zinc finger E-box binding homeobox 1 (*Zeb1*) and zinc finger binding homeobox 2 (*Zeb2*), and through reduced upregulation of epithelial markers such as E-cadherin (*E-cad*), epithelial cell adhesion molecule (*Epcam*), and *occludin* (Fig. 3F). To precisely estimate the change in MET, we used flow cytometry to assess the percentage of cells positive for both E-Cad and thymocyte differentiation antigen-1 (Thy-1) as a mesenchymal marker on day 6 of reprogramming in both *Alkbh5* WT and KO MEFs. Reprogramming of *Alkbh5* KO MEFs resulted in a reduced fraction of E-Cad positive cells as compared to WT MEFs, while we did not see any significant difference in the fraction of

Thy1 positive cells (Fig. 3G). Furthermore, to strengthen our findings, we repeated the same experiment using another mesenchymal marker, PDGFRβ, together with E-Cad, which clearly indicated a reduction in the fraction of the E-Cad positive cells on day 6 of reprogramming of *Alkbh5* KO MEFs as compared to WT MEFs, while we did not see any significant difference in the fraction of PDGFRβ positive cells (Fig. 3H). In addition, we used *Alkbh5*$^{f/f}$ MEFs and found that depletion of *Alkbh5* by using 4-OH Tam resulted in a reduction in the fraction of E-cad positive cells on day 6 of reprogramming, while we did not see any significant difference in the fraction of Thy1 or PDGFRβ positive cells (Supplementary Fig. 3T-V). It is noteworthy that the discrepancy between PDGFRβ RNA and protein levels might due to posttranscriptional regulation. Moreover, to gain more insight into MET in the context of reprogramming, we used flow cytometry to assess both SSEA1 and E-Cad positive populations on day 7 and 14 of reprogramming. Our data revealed that the SSEA1 positive population emerged from the E-Cad positive population, and *Alkbh5* KO MEFs showed a reduction in the percentage of both the single positive E-Cad population and double positive SSEA1/E-Cad population compared to WT MEFs on both day 7 and day 14 (Fig. 3I and supplementary Fig. 3W). Although ALKBH5-HA overexpression did not have any effect on MET or reprogramming efficiency on day 7, its overexpression in the late stage of reprogramming increased both the fraction of single positive E-Cad cells and the fraction of double positive SSEA1/E-Cad cells as compared to WT MEFs (Fig. 3I and supplementary Fig. 3W). In addition, we used Δ-PE-Oct4-GFP MEFs and flow cytometry to assess the E-Cad positive and Δ-PE-Oct4-GFP positive populations on day 14 of reprogramming. Our data revealed that the Δ-PE-Oct4-GFP positive population emerges from the E-Cad positive population and that knockdown of *Alkbh5* decreases both the fraction of E-Cad single positive cells and the fraction of double positive Δ-PE-Oct4-GFP/E-Cad cells as compared to the WT control (Supplementary Fig. 3X). The role of ALKBH5 in MET is further supported by our

observations of morphological changes during reprogramming after *Alkbh5* depletion (Supplementary Fig. 3Y). In summary, *Alkbh5* is required for proper cell proliferation and for proper upregulation of epithelial markers during the early phase of reprogramming.

Cyclin B1 and *B2* are downstream targets of ALKBH5.

Our data revealed that depletion of *Alkbh5* induced cell cycle arrest at G2/M phase, accompanied by a reduction in the expression of both *Cyclin B1* and *B2* (Fig. 3A-E). Next, we asked whether overexpression of CYCLIN B1 and/or B2 can compensate for *Alkbh5* depletion during reprogramming. We overexpressed CYCLIN B1 and B2 individually or together in both *Alkbh5* WT and KO MEFs (Fig. 4A and Supplementary Fig. 4A). We found that overexpression of either CYCLIN B1 or B2, or both together, enhanced cell proliferation in both *Alkbh5* WT and KO MEFs during reprogramming (Supplementary Fig. 4B). Then, we used Δ-PE-Oct4-GFP to assess the role of CYCLIN B1 and/or B2 in reprogramming. Our data revealed that overexpression of either CYCLIN B1 or B2, or both together, enhanced the reprogramming efficiency as measured by an increased number of GFP positive colonies and an increased fraction of Δ-PE-Oct4-GFP positive cells on day 14 of reprogramming (Fig. 4B, C). Furthermore, we applied ALP staining and flow cytometry to assess the fraction of SSEA1 positive cells on day 7 and day 14 of reprogramming in *Alkbh5* WT and KO MEFs overexpressing either CYCLIN B1 or B2, or both. Our data showed that overexpression of either CYCLIN B1 or B2, or both, enhanced the reprogramming efficiency in *Alkbh5* WT MEFs as assessed by an increased fraction of SSEA1 positive cells on day 7 and day 14 accompanied with increasing in the cell number (Supplementary Fig. 4B, C). Overexpression of either CYCLIN B1 or B2, or both, restored the fraction of SSEA1 positive cells in *Alkbh5* KO MEFs on day 7, while the reprogramming efficiency increased on day 14 compared to

control MEFs (Supplementary Fig.4B, C). Our ALP staining data showed that overexpression of either CYCLIN B1 or B2, or both, enhanced the reprogramming efficiency in both *Alkbh5* WT and KO MEFs (Supplementary Fig. 4D, E). To further explore the mechanism of *Cyclin B1* and *B2* regulation in the context of *Alkbh5* depletion, we assessed the turnover of *Cyclin B1* and *B2* during reprogramming of WT and KO *Alkbh5* MEFs. Our data showed that the stability of both *Cyclin B1* and *B2* were further reduced in *Alkbh5* KO MEFs compared to WT control during reprogramming (Fig. 4D). The reduction in *Cyclin B1* and *B2* stability in *Alkbh5* KO MEFs during reprogramming reflected the reduction in their expression at both the RNA and protein levels (Fig. 3D, E). Furthermore, we performed m6A-IP on day 3 of reprogramming, and our data revealed increased m6A enrichment on both *Cyclin B1* and *B2* in *Alkbh5* KO MEFs compared to WT MEFs (Fig. 4E). Taken together, our data suggest that increased m6A levels at *Cyclin B1* and *B2* results in decreased stability, hence reduced expression at both the RNA and protein level, leading to cell cycle arrest at G2/M phase and a reduction in reprogramming efficiency.

ALKBH5 overexpression in the late phase enhances reprogramming efficiency by upregulating *Nanog*

We assessed the impact of ALKBH5 overexpression on the reprogramming process. We used lentiviral expression to achieve high expression of both ALKBH5 and ALKBH5-HA during reprogramming (Fig. 5A). Our data revealed that overexpression of ALKBH5-HA enhanced the reprogramming efficiency by increasing the fraction of Δ-PE-Oct4-GFP positive cells and the number of GFP positive colonies as compared to the control (Fig. 5B, C). We further confirmed our data using flow cytometry to assess the fraction of SSEA1positive cells and ALP positive colonies. In agreement with our previous data (Supplementary Fig. 3V),

overexpression of either ALKBH5 or ALKBH5-HA enhanced the reprogramming process, as measured by an increase in the percentage of SSEA1 positive cells and an increase in the number of ALP positive colonies at day 14 of reprogramming (Fig. 5D, E). Moreover, overexpression of ALKBH5 and ALKBH5-HA increased both the E-Cad single-positive population and the Δ-PE-Oct4-GFP/E-Cad double-positive population compared to the control (Supplementary Fig. 5A). In addition, the percentage of the Δ-PE-Oct4-GFP positive cells gated on the SSEA1 positive population increased by overexpression of either ALKBH5 or ALKBH5-HA (supplementary Fig. 5B).

To investigate at what time ALKBH5 overexpression enhances reprogramming efficiency, we used a Dox inducible overexpression system. We did not find any significant effect of ALKBH5 overexpression on the reprogramming efficiency at the early phase from day 1 to day 7. However, the percentage of SSEA1 positive cells at day 14 was greatly increased after overexpression of ALKBH5-HA from day 1-14, as well as after overexpression from day 7-14 only (Fig. 5F). To determine the precise time point at which ALKBH5 overexpression has a positive impact on the reprogramming process, we used Dox-inducible overexpression of ALKBH5-HA in Δ-PE-Oct4-GFP MEFs to induce ALKBH5 expression at seven different time intervals (day 0-2; 2-4; 4-6; 6-8; 8-10; 10-12 and 12-14), and we estimated the reprogramming efficiency using Δ-PE-Oct4-GFP by flow cytometry on day 14. In agreement with our previous data (Fig. 5F and Supplementary Fig. 2D), ALKBH5-HA overexpression did not have any impact on the early phase of reprogramming, while the positive impact was observed from day 8 onwards (Supplementary Fig. 5C).

To investigate the molecular mechanism responsible for enhancing reprogramming efficiency by overexpression of ALKBH5 at the late phase, we used a Dox inducible system for temporal overexpression of ALKBH5 from day 10 to day 12 (Fig. 6A, B). We found that

overexpression of ALKBH5 resulted in upregulation of the endogenous RNA level of reprogramming factors such as *Oct4*, *Sox2* and *Klf4* and other pluripotency factors, including *Klf2, Tbx3, and Esrrb*, and in particular *Nanog* (Fig. 6B, C). We obtained similar results by overexpression of ALKBH5 from day 8 to day 10 (Supplementary Fig. 6A-C). Previous studies have reported that *Nanog* is regulated posttranscriptionally in both mouse and human ESCs by the m^6A machinery (Batista et al., 2014, Geula et al., 2015). We hypothesized that *Nanog* transcripts are posttranscriptionally regulated through the m^6A modification during reprogramming and that overexpression of the m^6A demethylase ALKBH5 will reduce m^6A levels, potentially affecting the stability of *Nanog* transcripts. To test this hypothesis in the reprogramming context, we performed m^6A IP at day 12 of reprogramming and indeed found that overexpression of ALKBH5 decreased the m^6A level at *Nanog* transcripts (Fig. 6D). Furthermore, we assessed the stability of *Nanog* transcripts after overexpression of ALKBH5. We found that overexpression of ALKBH5 resulted in increased stability of *Nanog* transcripts (Fig. 6E). Next, we assessed whether ALKBH5 overexpression could rescue the *Alkbh5* KO phenotype in reprogramming. Our data revealed that overexpressing either ALKBH5 or ALKBH5-HA in *Alkbh5* KO MEFs could restore the reprogramming efficiency (Supplementary Fig. 6D-G). Finally, we tested whether NANOG overexpression could compensate for *Alkbh5* knockdown. We used a Dox-inducible overexpression system to control NANOG overexpression during reprogramming (Supplementary Fig. 6H). Our data revealed that overexpression of NANOG enhanced reprogramming in both WT MEFs and *Alkbh5* knockdown MEFs as measured on day 14 as an increase in the fraction of Δ-PE-Oct4-GFP positive cells and the number of Δ-PE-Oct4-GFP positive colonies (Fig. 6F, G). Furthermore, overexpression of NANOG resulted in an increased fraction of SSEA1 positive cells in both WT and *Alkbh5* KD MEFs at day 14 of reprogramming (Supplementary Fig. 6I).

Taken together, our findings suggest that ALKBH5 overexpression in the late phase of reprogramming enhances reprogramming efficiency by decreasing the m^6A level at *Nanog* transcripts, thus stabilizing these transcripts and resulting in upregulation of *Nanog*. In addition, overexpression of NANOG can compensate for the negative effect *Alkbh5* depletion has on reprogramming efficiency.

Discussion

Ectopic expression of the four transcription factors OCT4, SOX2, KLF4, and c-MYC in somatic cells can establish the pluripotency regulatory circuitry, resulting in massive changes at both the epigenetic and transcriptional levels and the generation of iPSCs (Takahashi et al., 2007, Takahashi and Yamanaka, 2006). Successful therapeutic application of these iPSCs will likely require a comprehensive understanding of the molecular mechanism underlying somatic cell reprogramming. Here, we aimed to dissect the role of the m^6A demethylase ALKBH5 in somatic cell reprogramming.

Our data revealed that the catalytic activity of ALKBH5 is required for the regulation of the reprogramming process. Both catalytically inactive ALKBH5 (H205A) and catalytically deleted ALKBH5 (CD) overexpression failed to restore the reduced reprogramming efficiency in *Alkbh5* KO MEFs, and their overexpression in WT MEFs impaired the reprogramming efficiency and cell proliferation.

Resetting the pluripotency cell cycle pattern is an essential step of achieving successful iPSC generation, suggesting that the cell division rate is a key parameter for somatic cell reprogramming (Hanna et al., 2009). In agreement with that, *p53* and *Ink4/Arf* have been shown to act as barriers to the reprogramming process (Kawamura et al., 2009, Hong et al., 2009, Li et al., 2009). Additionally, G2/M cell cycle regulators have been

reported to maintain pluripotency, and the Cdk1/Cyclin B1 complex has been reported to enhance the reprogramming process (Gonzales et al., 2015, Wang et al., 2017). Moreover, the m^6A machinery has been reported to be involved in regulating Cdk1 and Cyclin B2, and knockout of Fat mass and obesity-associated (*Fto*) results in decreased expression of Cdk1 and Cyclin B2, causing G2/M cell cycle arrest in spermatogonia (Huang et al., 2019). Here, we showed that *Alkbh5* depletion in MEFs or during the early phase of somatic cell reprogramming decreased the expression of Cyclin B1 and B2 accompanied by cell cycle arrest at G2/M phase, which in turn resulted in reduced proliferation and MET transformation rate, ultimately leading to impaired reprogramming efficiency. Overexpression of either CYCLIN B1 or B2, or both, restored the phenotype of *Alkbh5* depletion and additionally enhanced the reprogramming process. However, we do not rule out that other mechanisms may also be at play, e.g. we acknowledge that we cannot formally exclude the possibility that *Alkbh5* might have a direct effect on MET. This could be an interesting point for future studies. Furthermore, future work, including m6A-IP-seq, could provide new candidates downstream of ALKBH5 that might overlap with the functional role of CYCLIN B1 or B2 in regulating G2/M phase during reprogramming.

Moreover, in contrast with that observed for the early phase of reprogramming, we found that depletion of *Alkbh5* in the late phase of reprogramming did not have a significant effect on reprogramming efficiency. This indicates that the negative effect of *Alkbh5* depletion on reprogramming efficiency occurs specifically during the early phase, where both resetting of the cell cycle pattern and morphological transformation to epithelial-like cells occur.

Recent studies have revealed that the m^6A modification on mRNA is essential in regulating pluripotency, self-renewal of stem cells, somatic cell reprogramming, and early embryonic development (Chen et al., 2015, Aguilo et al., 2015). Regulation of pluripotency

by the m^{6}A machinery has been reported in both mouse and human ESCs, where *Mettl3* and/or *Mettl14* depletion induces a hyper-pluripotent state, presumably through increasing the m^{6}A level at several pluripotency related transcripts, such as *Nanog*, resulting in increased transcript stability that hinders cells from exiting the pluripotency state (Geula et al., 2015, Batista et al., 2014). NANOG is a key regulator of pluripotency and is required for acquiring pluripotency during the late phase of reprogramming (Pan and Thomson, 2007, Silva et al., 2009). A synergistic role of NANOG in overexpression together with DNA demethylation agents in the late phase of reprogramming has been reported to enhance acquisition of the pluripotency state (Theunissen et al., 2011, Silva et al., 2009). Moreover, NANOG co-binds with OCT4, SOX2 and KLF4 to many regulatory regions to facilitate the binding of the coactivator P300 (Chen et al., 2008). Here, we showed that ALKBH5 overexpression in the late phase of reprogramming decreases the m^{6}A level at *Nanog* transcripts, resulting in increased *Nanog* stability and enhanced reprogramming efficiency. Overexpression of NANOG enhances the reprogramming efficiency in both WT and *Alkbh5* knockdown MEFs. Consistent with our findings, ALKBH5 has been reported to positively regulate *Nanog* stability and expression in response to hypoxia-inducible factor (HIF)-1α and HIF-2α in breast cancer stem cells (BCSCs) (Zhang et al., 2016).

A recent study reported that YTHDF2/3, but not YTHDF1, regulates MET events in somatic cell reprogramming in an m^{6}A dependent manner through the Hippo signaling pathway effector *Tead2* (Liu et al., 2020). Other studies have shown redundancy among the three paralogs *Ythdf1/2/3*, suggesting that they can have adequate functional compensation, at least in some biological contexts (Zaccara and Jaffrey, 2020, Lasman et al., 2020). It would be interesting to assess the role of *Ythdf1/2/3*, as well as any redundancy, in the context of *Alkbh5* depletion in future studies.

In conclusion, we provide mechanistic insight into the epitranscriptional regulation of somatic cell reprogramming by elucidating the biphasic regulatory role of ALKBH5 in modulating reprogramming efficiency at the posttranscriptional level in a stage specific manner (Fig. 7).

Materials and Methods

MEFs derivation

All of Wild type (WT), Knockout (KO) *Alkbh5* and homozygous floxed *Alkbh5* MEFs (*Alkbh5*$^{f/f}$) were derived from embryos at 13.5 d.p.c. Mice were housed and mated in Norwegian Transgenic Center (NTS). Briefly, pregnant C57BL/6 female mice were sacrificed on 13.5 or and embryos were dissected. The internal organs, head, and limbs were removed and used for genotyping. Then the remaining tissues were trypsinized using 0.25% trypsin for 30 min at 37^{0}C with shaking to make single cell suspensions, then cells were pooled and plated in MEFs media until 80% confluence then trypsinized and stored in freezing solution (FBS+10% DMSO) in liquid nitrogen for future use. MEFs were cultured and maintained in DMEM+10% FBS (tetracycline free FBS PAN-Biotech Catalog # P30-2602TC) till reaching to 70%-80% confluence, then passaged at 1x10^5 cells per well of 6-well plate.

Alkbh5$^{f/f}$ MEFs were plated at 1x10^5 cells per well of 6-well plate overnight. Next day the cells were transfected with KA1153 pPB-CAG-MerCreMer-IN (Addgene Plasmid #124183) together with PBase (Guo et al., 2009), and PB-CAG-HA-IRES-Puro (a kind gift from professor Hitoshi Niwa , Kumamoto University IMEG) using Lipofectamin 2000 (Invitrogen# 11668019) or Fugene 6 (Promega #E2691). The medium was changed after 5 hours. Next day, the cells were cultured with medium containing 2µg/ml of Puromycin (Fisher Scientific # A1113803) for 2 days. Then cells were treated with 1µM of 4 Hydroxy

Tamoxifen (4-OH Tam) (Merk#H7904-5MG) for depletion of *Alkbh5* at indicated time points. Cells are routinely tested and are mycoplasma free.

Reprogramming

For reprogramming MEFs at early passages were plated as single cells at $1x10^5$ per well of 6 well plate or 5-6 $x10^5$/ 10 cm dish depending on the purpose of experiment. The cells were infected with equal ratio of the retroviruses expressing the four reprogramming factors (Oct4, Sox2, Klf4, and c-Myc) and incubated at 37^0C for 8-12 hours with 8 µg/ml of polybrene. The medium was changed next day. For either knockdown or overexpression experiments during reprogramming, the MEFs were plated at $1x10^5$ per well of 6 well, and infected with lentivirus for 8 hours, them medium was changed, and next day the selectable markers were added for 2 days. If the cells were trypsinized at day 7 reprogramming, the reprogrammed cells cultured with feeder layer CF-1 MEFs Irradiated, P3 2M (AMS biotechnology #GSC-6201G 2M or #GSC-6101G 7M) and LIF ESGRO® Recombinant Mouse LIF Protein (1000 units/mL) (Millipore # ESG1107). For induction of the transgene Stemolecule Doxycycline hyclate 10 mg (Stemgent#04-0016) was added at 1µg/ml every 2 days. OG2 was a kind gift from Professor Hans R. Schöler (Velychko et al., 2019) . The reprogramming efficiency was checked on day 14 by flow cytometry.

Piggybac reprogramming protocol was used as previously described (Kim et al., 2015). Briefly MEFs were seeded in $1x10^5$ cells per 10 cm dish (multiple dishes were used in parallel) overnight. Next day as mixture of 500 ng of PB-TAC-OSKM vector obtained from Addgene (Plasmid #80481), 500 ng of pPB-CAG-rtTA-IN (Plasmid #60612), and 1000 ng of piggybase plasmid at a Fugene/DNA ratio of 4 µL: 1 µg DNA. Next day, the medium was changed with dox at concentration 1µg/ml for 1 day. Next day, cells were checked for

mcherry positive and seeded in multiple wells of 6 well plate at density $1x10^4$ cells. The reprogrammed cells were checked by flow cytometry at day 7 and day 14 of with both mcherry and SSEA1-Alexa 488.

Both WT and KO Alkbh5 MEFs were seeded in $1x10^5$ cells per well of 6 well plate and infected with equimolar ratio of OSKM retrovirus and lentiviral of both FUW-M2rtTA Addgene (Plasmid #20342) and FUW-TetO-Nanog Addgene (Plasmid #40800) . On day 7 of reprograming for dox was added at concentration 1µg/ml and cells were checked for reprogramming efficiency at day 14 by flow cytometry.

Retrovirus preparation

Plate E cells were used for preparation of retrovirus (Cell bio labs #RV-101) Plate E cells were plated at $1x10^6$ cells per 10 cm dish in DMEM+ %10 FBS (tetracycline free FBS PAN-Biotech Catalog # P30-2602TC) till reaching to 70% to 80% confluence. Then cells were transfected with 9 µg of each of pMXs-Oct4 (Addgene Plasmid #13366), pMXs-Sox2 (Addgene Plasmid #13367), pMXs-Klf4 (Addgene Plasmid #13370), pMXs-c-Myc (Addgene Plasmid #13375) per 10 cm dish using Fugene 6 (Catalog# Promega# E2691), and the medium was changed after 8 hours using (IMEDM+10%FBS). Retroviral supernatant were harvested after 48 and 72 hours and centrifuged at 1200 r.p.m for 5 minutes at 4ºC. The retroviral supernatant was used freshly or frozen in aliquots at -80ºC. The viral titer was estimated to produce up to 7-8% SSEA1 on day 7 of reprogramming or using GFP control estimated more than 85% infection efficiency by FACS.

Lentivirus preparation

Lenti-X 293T cells were used for preparation of lentivirus (Takahara Clontech #632180). Lenti-X 293T cells were plated at $1x10^6$ cells per 10 cm dish in DMEM+ %10 FBS (tetracycline free FBS) till the cells reach 70% - 80% confluence . The cells were transfected with PsPAx2 (Addgene Plasmid #12260), pMD2.G (Addgene Plasmid #12259), and the vector encoding either shRNA for Knockdown *Alkbh5* or overexpression either ALKBH5, ALKBH5-HA, ALKBH5-HA (H205A), ALKBH5-HA (CD), NANOG, CYCLIN B1 or B2 using Fugene 6. The medium was changed after 8 hours using (IMEDM+10%FBS). Lentiviral supernatant were harvested after 48 and 72 hours and centrifuged at 1200 r.p.m for 5 minutes at 4^0C.The lentiviral supernatant was used freshly or frozen in concentrated aliquots using Lenti-X™ Concentrator Takahara catalog number #631232) and stored at -80^0C.

Cell proliferation assay

Mouse embryonic fibroblasts (MEFs) were plated at $1x10^4$ per well of 24 well plate at quadruplicate. Then, at each indicated time point four wells were trypsinized and counted independently using (Life Technologies #C10228 Countess™ Cell Counting Chamber Slides). Medium was replaced every 2 days and the data are presented as mean±SD for quadruplicate samples.

For reprogramming experiment, MEFs were plated at $1x10^5$ cells per well of 6-well plate in triplicate, and infected with equal molar ratio of retroviral titer encoding Oct4, Sox2, Klf4, and c-Myc with or without pMXs-DsRed was obtained from Addgene (Plasmid #22724) as a control for 6 hours then medium changed. Almost 8 hours after infection, cells were treated with either ethanol or 1μM of 4-hydroxy- Tamoxifen (4-OH-Tam) for depletion of

Alkbh5. Cells were trypsinized at indicated time points and counted. Medium was replaced every 2 days and the data are presented as mean±SD for triplicate samples.

Genotyping

Cells of tissue biopsies has been suspended in lysis buffer (1M Tris-PH 8, 5M NaCl, 0.5M EDTA PH8, 10% SDS) and freshly added (Proteinase K 20mg/ml) and incubated at 37^0C for 4hrs to overnight. Then 300µl of 5M NaCl was added followed by vortexing and incubation on ice for 10 min then spinning at low speed. Then the supernatant was removed and transferred to new tube followed by 650µl Iso-propanol and vortexing, and incubation at RT for 15 min, then centrifugation at 150,000 r.p.m. Then the supernatant was discarded and the pellet was dissolved in 200µl TE buffer, followed by incubation at 55^0C for 10 min, then the DNA concentration is measured and 10-50 ng was used per reaction.

Cloning

Both mALKBH5 and mALKBH5-HA were amplified from the cDNA using gateway forward and reverse primer using PrimeSTAR GXL DNA Polymerase (Takahara Clontech # R050A-TAK). The PCR product was purified using QIAquick PCR Purification Kit (Qiagen #28106), then shuttled to Gateway™ pDONR™221 Vector (Invitrogen#12536017) using Gateway™ BP Clonase™ II Enzyme mix (Invitrogen#11789020). Then the construct was transformed to One Shot™ Stbl3™ Chemically Competent E. coli (Thermo Fisher #C737303). Positive clones were screen by colony PCR and restriction digestion then positive colonies were sent for sequencing. The correct clone was used as entry clone and then the construct was shuttled to destination vector pLX301 (Addgene Plasmid #25895) For

constitutive overexpression of either ALKBH5 or ALKBH5-HA, and pCW57.1 (Addgene Plasmid #41393) for dox inducible overexpression using LR clonase (Thermo #11791020) based on manufacture protocol. Then transformed to Stbl3 competent cells in case of Lentiviral destination vector. Then colonies were screened by colony PCR and restriction digestion. The positive colonies were sent for sequencing and the correct colony was propagated and the plasmids were purified using Qiagen (Endotoxin free kit #12362), and used for making the virus.

For shRNA cloning

Two short hairpins shRNA for targeting *mAlkbh5* were annealed in annealing buffer by heating for 10 minutes at 95^0C in thermocycler then cooling by gradual decreasing the temperature to 4^0C for 30 minutes. Then the annealed oligos were ligated using T4 DNA Ligase (5 U/µL) (Thermo Fisher Scientific #EL0011) to either pLKO.1 puro (Addgene Plasmid #8453) for constitutive knockdown or Tet-pLKO-puro (Addgene Plasmid #21915) for dox inducible knockdown which was linearized with AgeI-HF (NEB # R3552L) and EcoRI-HF (NEB#R3101S) restriction enzymes. Then the ligated product was transformed to One Shot™ Stbl3™ Chemically Competent E. coli (Thermo Fisher #C737303). Several colonies were picked up and sent for sequencing. The positive clones were propagated and the plasmid was purified using Qiagen (Endotoxin free kit #12362) and used for making the virus.

Both pENTR vector encoding both *Cyclin B1* (Plasmid #136340) and *B2* (Plasmid #136341) were obtained from addgenea. Then the construct was shuttled through gateway cloning system using LR clonase into pMXs-GW (Plasmid #18656) retroviral vector. Then several colonies were picked up and correct colonies were confirmed by colony PCR and

sequencing. Then positive colony was propagated and the plasmids were purified using Qiagen (Endotoxin free kit #12362), and used for making the retrovirus.

The pDONR™221 vector encoding *mAlkbh5-HA* tag used as template for making both point mutation (H205A) ALKBH5-HA and catalytic deletion (CD) ALKBH5-HA using combination of overlap extension PCR and Q5® Site-Directed Mutagenesis Kit (NEB# E0554S) with the primers listed in (table 1) based on the manufacturer protocol with some modifications. And the positive colonies were confirmed by colony PCR and sequencing. Then positive colony was used to shuttle the construct to either to destination vector pLX301 and pCW57.1 using LR clonase based on manufacturer protocol. Then positive colony was propagated and the plasmids were purified using Qiagen (Endotoxin free kit #12362), and used for making the lentivirus.

qPCR

TRIzol™ LS Reagent (Thermo scientific 10296010) was used for RNA extraction according to the manufacturer protocol, then the RNA was dissolved in UltraPure™ DNase/RNase-Free Distilled Water (Thermo Scientific 10977049), then 1µg was used to make the cDNA using SuperScript™ IV VILO™ Master Mix with ezDNase™ Enzyme (Thermo Scientific 11766050) based on manufacturer protocol. For Real time PCR, 2µl of cDNA was used per reaction using PowerUp™ SYBR™ Green Master Mix (Thermo Scientific A25777). The transcript level was normalized to the internal control**.** List of primers is attached in (Supplementary table 1).

RNA stability

Cells were treated with 5µg/ml of Actinomycin D (Tocris #1229) for indicted time point 3, 6, and 9 hours. Total RNA was extracted at each time point. DMSO treated cells was used as a control, and relative RNA expression was detected by qPCR

m6A dot blot

Total RNA was extracted from cells using TRIzol™ LS Reagent (Thermo scientific 10296010) or RNeasy Plus Mini Kit (Qiagen# 74134). mRNA was isolated and purified using Dynabeads™ mRNA Purification Kit (for mRNA purification from total RNA preps) (Invitrogen # 61006) following the manufacturer's instructions. For m6A dot blot, mRNA was hybridized onto the Hybond-N+ membrane (GE Healthcare). After crosslinking spotted mRNA to membrane using Stratalinker 2400 UV Crosslinker, the membrane was blocked with 5% skimmed milk for 1 h, incubated with mouse anti-m6A antibody (1:1000, Millipore # MABE1006) at 4°C overnight. Then the membrane was incubated with HRP-conjugated donkey anti-mouse IgG at room temperature for 1 h. The membrane was photographed using the ECL imaging system (Bio-Rad). Finally, the membrane was stained with 0.02% methylene blue. Relative m6A level was quantified using ImageJ.

m6A IP-qPCR

Control and Alkbh5-HA overexpressed reprogrammed cells at day 12 of reprogrammed were harvested and mRNA was extracted from RNA as described previously. 1 to 2 µg of mRNA was fragmented at 70^0c for 4 minutes. The mRNA was precipitated and the pellet was dissolved in Ultrapure DNase/RNase free water, then incubated with pre

conjugated m6A/protein G (Dynabeads™ Protein G for Immunoprecipitation#10003) beads in IP buffer, and incubated at 4^0C for overnight. The mRNA was isolated from the beads using Trizol LS, and the RNA was used to make cDNA using SuperScript™ IV VILO™ Master Mix with ezDNase™ Enzyme (Thermo Scientific 11766050) based on manufacturer protocol . The m6A mRNA level was finally determined by real-time quantitative PCR relative to the input.

Western blot

Cells were washed twice with ice cold 1xPBS, and then scrapped and transferred to 1.5 ml Eppendorf tube, then centrifuged and supernatant was discarded. The cells were lysed on RIPA lysis buffer (20mM Tris-HCl PH7.5, 1mM MgCl2, 500mM NaCl, 20% glycerol ,0.5% NP-40, 1mM EDTA, 1mM EGTA) and freshly added 1x Halt Protease Inhibitor cocktail (100X) (Thermo Fisher #87786) and incubated on ice for 30 min. The lysed cells centrifuged at maximum speed for 30 minutes and the supernatant was transferred to new Eppendorf. Then protein content was measured using Bradford protein assay (BSA) method and then equal amounts of protein was lysed with 1x Bolt™ LDS Sample Buffer (Thermo Scientific B0008) and 1x Bolt™ Sample Reducing Agent (Thermo Scientific B0009). The sample loaded on Bolt ready gel (4-12%) and transferred to PVDF or nitrocellulose Biorad pads using Trans-Blot Turbo Transfer System. Then the membrane was blocked using 5% skimmed milk in 1xTBST buffer and then incubated with the primary antibody overnight. Next day, the membrane was washed 3 times using 1xTBST buffer and incubated with the secondary antibody for 1 hr at RT. The membrane was washed 3 times using 1xTBST buffer, and then the protein detected with Pierce™ ECL Western Blotting Substrate (Thermo Fisher 32209) or SuperSignal™ West Femto Maximum Sensitivity Substrate (Thermo Fisher

34094), using Biorad ChemiDoc XRS, and Precision Plus Protein™ Dual Color Standards (Bio-Rad#161-0374) as a protein standard. Antibodies list is attached (Supplementary table 2). The raw data of western blot were included in (supplementary Fig. 7).

Alkaline phosphatase staining

Alkaline phosphatase staining was done using Leukocyte Alkaline Phosphatase Kit (Sigma 85L3R) based on the manufacturer protocol as previously described (Khodeer and Era, 2017).

Cell cycle analysis

The cells were trypsinized and washed 2 times with 1xPBS. Then the cells was suspended in 300µl ice cold 1xPBS and 700µl of ice cold 100% ethanol was added drop by drop with vortexing. The cells were incubated at 4ºC for at least 30 minutes. Then the cells were centrifuged and the pellet was suspended in 200µl (Propidium Iodide (PI)/RNase Staining Solution (Cell signaling 4087S) and incubated at RT for 30 minutes before analysis by FACS.

Apoptosis

Detection of apoptotic cells was done by using FITC-Annexin V Apoptosis Detection Kit with 7-AAD (Biolegend#640922). Briefly, the cells were collected and washed 2 times with 1xPBS. The cells were suspended in 200µ 1x binding buffer, 1µl Annexin V- FITC, and

7AAD (1:200). The cells were incubated at RT for 30 minutes in the dark. The cells were centrifuged and suspended in 300µl 1x binding buffer and then analyzed by FACS. G

SSEA1 staining

Cells at indicated time points were washed two times with 1xPBS then trypsinized. The cells were counted and $1x10^6$ cells were washed again with 1x Hanks buffer and stained with 5µl of Alexa Fluor® 647 anti-mouse/human CD15 (SSEA-1) Antibody (Biolegend#125608) or SSEA1-Alexa 488 (Biolegend # 125610) in100µl BD Pharmingen™ Stain Buffer (FBS) (BD Biosciences #554656) for 30 min on Ice. The cells were washed once with 1x Hanks buffer and stained with 7AAD (1:200). The SSEA1 positive fraction was analyzed using FACS BD Fortessa. For the MET checking, the cells at indicated time points were washed two times with 1xPBS then trypsinized. The cells were counted and $1x10^6$ cells were washed again with 1x Hanks buffer and double stained with either Thy1-Pacific blue (Biolegend # 140306) and E-Cad Alexa 647(Biolegend #147308) or PDGFRβ-APC (Biolegend #136008) and E-Cad Brilliant Violet 421 (Biolegend #147319).

BrdU incorporation assay

APC BrdU Flow Kit (BD Biosciences #552598) was used according to the manufacturer's protocol. Briefly, cells were labeled by adding 10 µM of BrdU to the culture medium. Treatment was done for 1 hour and then cells were fixed and permeabilized. Then cells were treated with DNase for 1 hour at 37^0c. Then stained with anti-BrdU APC for 20 minutes at RT then resuspended in 7AAD and analyzed by FACS.

Statistical Analysis

All data were collected from at least three independent experiments. Data were analyzed using Student's *t*-test or one-way ANOVA followed using Graphpad software. Significance was presented as $^{*}p < 0.05$, $^{**}p < 0.01$, and $^{***}p < 0.001$. Error bars represented mean±SD.

GUO, G., YANG, J., NICHOLS, J., HALL, J. S., EYRES, I., MANSFIELD, W. & SMITH, A. 2009. Klf4 reverts developmentally programmed restriction of ground state pluripotency.

KIM, S.-I., OCEGUERA-YANEZ, F., HIROHATA, R., LINKER, S., OKITA, K., YAMADA, Y., YAMAMOTO, T., YAMANAKA, S. & WOLTJEN, K. 2015. KLF4 N-terminal variance modulates induced reprogramming to pluripotency. *Stem Cell Reports,* 4**,** 727-743.

VELYCHKO, S., ADACHI, K., KIM, K.-P., HOU, Y., MACCARTHY, C. M., WU, G. & SCHÖLER, H. R. 2019. Excluding Oct4 from Yamanaka cocktail unleashes the developmental potential of iPSCs. *Cell Stem Cell,* 25**,** 737-753. e4.

Acknowledgments

The authors thank the Norwegian Transgenic Center (Norsk Transgen Senter (NTS)) and, in particular, Shiasta Khan, Ingunn Jermstad, and Dr. Knut Tomas Dalen for setting up and maintaining floxed *Alkbh5* mouse mating and Guro Flor Lien and Gaute Nesse for maintaining and genotyping knockout *Alkbh5* mice. We are grateful to Professor Hans R. Schöler (Department of Cell and Developmental Biology, Max Planck Institute for Molecular) for providing us with OG2 MEFs. We would also like to thank Professor Hitoshi Niwa (IMEG, Kumamoto University) for supporting us with PBase and PB-CAG-HA-IRES-Puro.

Footnotes

Author contributions

S.K. and J.A.D. discussed and designed the study. S.K designed all experiments. S.K performed the experiments and analyzed the data. J.A.D. supervised the work. A.K. supervised mouse mating and contributed the mice. S.K wrote the first draft of the manuscript

and J.A.D revised and edited it. A.K. read and commented on the manuscript. All authors read and approved the final manuscript.

Disclosure of potential conflicts of interest

The authors declare they have no potential conflicts of interest.

Funding

This work was supported by the Helse Sør-Øst RHF Grant 2018063 and by the Norges Forskningsråd Grant 289467 for Young Research Talents Grant (to John Arne Dahl).

References

AGUILO, F., ZHANG, F., SANCHO, A., FIDALGO, M., DI CECILIA, S., VASHISHT, A., LEE, D.-F., CHEN, C.-H., RENGASAMY, M. & ANDINO, B. 2015. Coordination of m6A mRNA methylation and gene transcription by ZFP217 regulates pluripotency and reprogramming. *Cell stem cell,* 17**,** 689-704.

ALARCÓN, C. R., LEE, H., GOODARZI, H., HALBERG, N. & TAVAZOIE, S. F. 2015. N 6-methyladenosine marks primary microRNAs for processing. *Nature,* 519**,** 482-485.

BANITO, A., RASHID, S. T., ACOSTA, J. C., LI, S., PEREIRA, C. F., GETI, I., PINHO, S., SILVA, J. C., AZUARA, V. & WALSH, M. 2009. Senescence impairs successful reprogramming to pluripotent stem cells. *Genes & development,* 23**,** 2134-2139.

BATISTA, P. J., MOLINIE, B., WANG, J., QU, K., ZHANG, J., LI, L., BOULEY, D. M., LUJAN, E., HADDAD, B. & DANESHVAR, K. 2014. m6A RNA modification controls cell fate transition in mammalian embryonic stem cells. *Cell stem cell,* 15**,** 707-719.

BOKAR, J., SHAMBAUGH, M., POLAYES, D., MATERA, A. & ROTTMAN, F. 1997. Purification and cDNA cloning of the AdoMet-binding subunit of the human mRNA (N6-adenosine)-methyltransferase. *Rna,* 3**,** 1233-1247.

BUGANIM, Y., FADDAH, D. A., CHENG, A. W., ITSKOVICH, E., MARKOULAKI, S., GANZ, K., KLEMM, S. L., VAN OUDENAARDEN, A. & JAENISCH, R. 2012. Single-cell expression analyses during cellular reprogramming reveal an early stochastic and a late hierarchic phase. *Cell,* 150**,** 1209-1222.

CAREY, B. W., MARKOULAKI, S., HANNA, J. H., FADDAH, D. A., BUGANIM, Y., KIM, J., GANZ, K., STEINE, E. J., CASSADY, J. P. & CREYGHTON, M. P. 2011. Reprogramming factor stoichiometry influences the epigenetic state and biological properties of induced pluripotent stem cells. *Cell stem cell,* 9**,** 588-598.

CHAO, Y., SHANG, J. & JI, W. 2020. ALKBH5-m6A-FOXM1 signaling axis promotes proliferation and invasion of lung adenocarcinoma cells under intermittent hypoxia. *Biochemical and biophysical research communications,* 521**,** 499-506.

CHEN, T., HAO, Y.-J., ZHANG, Y., LI, M.-M., WANG, M., HAN, W., WU, Y., LV, Y., HAO, J. & WANG, L. 2015. m6A RNA methylation is regulated by microRNAs and promotes reprogramming to pluripotency. *Cell stem cell,* 16**,** 289-301.

CHEN, X., XU, H., YUAN, P., FANG, F., HUSS, M., VEGA, V. B., WONG, E., ORLOV, Y. L., ZHANG, W. & JIANG, J. 2008. Integration of external signaling pathways with the core transcriptional network in embryonic stem cells. *Cell,* 133**,** 1106-1117.

CHIN, M. H., MASON, M. J., XIE, W., VOLINIA, S., SINGER, M., PETERSON, C., AMBARTSUMYAN, G., AIMIUWU, O., RICHTER, L. & ZHANG, J. 2009. Induced pluripotent stem cells and embryonic stem cells are distinguished by gene expression signatures. *Cell stem cell,* 5**,** 111-123.

DENG, J., SHOEMAKER, R., XIE, B., GORE, A., LEPROUST, E. M., ANTOSIEWICZ-BOURGET, J., EGLI, D., MAHERALI, N., PARK, I.-H. & YU, J. 2009. Targeted bisulfite sequencing reveals changes in DNA methylation associated with nuclear reprogramming. *Nature biotechnology,* 27**,** 353-360.

DOMINISSINI, D., MOSHITCH-MOSHKOVITZ, S., SCHWARTZ, S., SALMON-DIVON, M., UNGAR, L., OSENBERG, S., CESARKAS, K., JACOB-HIRSCH, J., AMARIGLIO, N. & KUPIEC, M. 2012. Topology of the human and mouse m 6 A RNA methylomes revealed by m 6 A-seq. *Nature,* 485**,** 201-206.

GERKEN, T., GIRARD, C. A., TUNG, Y.-C. L., WEBBY, C. J., SAUDEK, V., HEWITSON, K. S., YEO, G. S., MCDONOUGH, M. A., CUNLIFFE, S. & MCNEILL, L. A. 2007. The obesity-associated FTO gene encodes a 2-oxoglutarate-dependent nucleic acid demethylase. *Science,* 318**,** 1469-1472.

GEULA, S., MOSHITCH-MOSHKOVITZ, S., DOMINISSINI, D., MANSOUR, A. A., KOL, N., SALMON-DIVON, M., HERSHKOVITZ, V., PEER, E., MOR, N. & MANOR, Y. S. 2015. m6A mRNA methylation facilitates resolution of naïve pluripotency toward differentiation. *Science,* 347**,** 1002-1006.

GONZALES, K. A. U., LIANG, H., LIM, Y.-S., CHAN, Y.-S., YEO, J.-C., TAN, C.-P., GAO, B., LE, B., TAN, Z.-Y. & LOW, K.-Y. 2015. Deterministic restriction on pluripotent state dissolution by cell-cycle pathways. *Cell,* 162**,** 564-579.

GUENTHER, M. G., FRAMPTON, G. M., SOLDNER, F., HOCKEMEYER, D., MITALIPOVA, M., JAENISCH, R. & YOUNG, R. A. 2010. Chromatin structure and gene expression programs of human embryonic and induced pluripotent stem cells. *Cell stem cell,* 7**,** 249-257.

HANNA, J., SAHA, K., PANDO, B., VAN ZON, J., LENGNER, C. J., CREYGHTON, M. P., VAN OUDENAARDEN, A. & JAENISCH, R. 2009. Direct cell reprogramming is a stochastic process amenable to acceleration. *Nature,* 462**,** 595.

HONG, H., TAKAHASHI, K., ICHISAKA, T., AOI, T., KANAGAWA, O., NAKAGAWA, M., OKITA, K. & YAMANAKA, S. 2009. Suppression of induced pluripotent stem cell generation by the p53–p21 pathway. *Nature,* 460**,** 1132-1135.

HUANG, T., GAO, Q., FENG, T., ZHENG, Y., GUO, J. & ZENG, W. 2019. FTO knockout causes chromosome instability and G2/M arrest in mouse GC-1 cells. *Frontiers in genetics,* 9**,** 732.

JIA, G., FU, Y., ZHAO, X., DAI, Q., ZHENG, G., YANG, Y., YI, C., LINDAHL, T., PAN, T. & YANG, Y.-G. 2011. N 6-methyladenosine in nuclear RNA is a major substrate of the obesity-associated FTO. *Nature chemical biology,* 7**,** 885-887.

KAWAMURA, T., SUZUKI, J., WANG, Y. V., MENENDEZ, S., MORERA, L. B., RAYA, A., WAHL, G. M. & BELMONTE, J. C. I. 2009. Linking the p53 tumour suppressor pathway to somatic cell reprogramming. *Nature,* 460**,** 1140-1144.

KIM, E. J., ANKO, M.-L., FLENSBERG, C., MAJEWSKI, I. J., GENG, F.-S., FIRAS, J., HUANG, D. C., VAN DELFT, M. F. & HEATH, J. K. 2018. BAK/BAX-mediated apoptosis is a Myc-induced Roadblock to reprogramming. *Stem cell reports,* 10**,** 331-338.

KIM, S.-I., OCEGUERA-YANEZ, F., HIROHATA, R., LINKER, S., OKITA, K., YAMADA, Y., YAMAMOTO, T., YAMANAKA, S. & WOLTJEN, K. 2015. KLF4 N-terminal variance modulates induced reprogramming to pluripotency. *Stem Cell Reports,* 4**,** 727-743.

LASMAN, L., KRUPALNIK, V., VIUKOV, S., MOR, N., AGUILERA-CASTREJON, A., SCHNEIR, D., BAYERL, J., MIZRAHI, O., PELES, S. & TAWIL, S. 2020. Context-dependent functional compensation between Ythdf m6A reader proteins. *Genes & development,* 34**,** 1373-1391.

LI, H., COLLADO, M., VILLASANTE, A., STRATI, K., ORTEGA, S., CAÑAMERO, M., BLASCO, M. A. & SERRANO, M. 2009. The Ink4/Arf locus is a barrier for iPS cell reprogramming. *Nature,* 460**,** 1136-1139.

LI, R., LIANG, J., NI, S., ZHOU, T., QING, X., LI, H., HE, W., CHEN, J., LI, F. & ZHUANG, Q. 2010. A mesenchymal-to-epithelial transition initiates and is required for the nuclear reprogramming of mouse fibroblasts. *Cell stem cell,* 7**,** 51-63.

LIU, J., GAO, M., XU, S., CHEN, Y., WU, K., LIU, H., WANG, J., YANG, X., WANG, J. & LIU, W. 2020. YTHDF2/3 are required for somatic reprogramming through different RNA deadenylation pathways. *Cell Reports,* 32**,** 108120.

LIU, J., YUE, Y., HAN, D., WANG, X., FU, Y., ZHANG, L., JIA, G., YU, M., LU, Z. & DENG, X. 2014. A METTL3–METTL14 complex mediates mammalian nuclear RNA N 6-adenosine methylation. *Nature chemical biology,* 10**,** 93-95.

MOR, N., RAIS, Y., SHEBAN, D., PELES, S., AGUILERA-CASTREJON, A., ZVIRAN, A., ELINGER, D., VIUKOV, S., GEULA, S. & KRUPALNIK, V. 2018. Neutralizing Gatad2a-Chd4-Mbd3/NuRD complex facilitates deterministic induction of naive pluripotency. *Cell stem cell,* 23**,** 412-425. e10.

OKITA, K., HONG, H., TAKAHASHI, K. & YAMANAKA, S. 2010. Generation of mouse-induced pluripotent stem cells with plasmid vectors. *Nature protocols,* 5**,** 418-428.

ONDER, T. T. & DALEY, G. Q. 2012. New lessons learned from disease modeling with induced pluripotent stem cells. *Current opinion in genetics & development,* 22**,** 500-508.

PAN, G. & THOMSON, J. A. 2007. Nanog and transcriptional networks in embryonic stem cell pluripotency. *Cell research,* 17**,** 42-49.

PING, X.-L., SUN, B.-F., WANG, L., XIAO, W., YANG, X., WANG, W.-J., ADHIKARI, S., SHI, Y., LV, Y. & CHEN, Y.-S. 2014. Mammalian WTAP is a regulatory subunit of the RNA N6-methyladenosine methyltransferase. *Cell research,* 24**,** 177-189.

RAIS, Y., ZVIRAN, A., GEULA, S., GAFNI, O., CHOMSKY, E., VIUKOV, S., MANSOUR, A. A., CASPI, I., KRUPALNIK, V. & ZERBIB, M. 2013. Deterministic direct reprogramming of somatic cells to pluripotency. *Nature,* 502**,** 65-70.

SAMAVARCHI-TEHRANI, P., GOLIPOUR, A., DAVID, L., SUNG, H.-K., BEYER, T. A., DATTI, A., WOLTJEN, K., NAGY, A. & WRANA, J. L. 2010. Functional genomics reveals a BMP-driven mesenchymal-to-epithelial transition in the initiation of somatic cell reprogramming. *Cell stem cell,* 7**,** 64-77.

SCHWARTZ, S., MUMBACH, M., JOVANOVIC, M., WANG, T., MACIAG, K., BUSHKIN, G., MERTINS, P., TER-OVANESYAN, D., HABIB, N. & CACCHIARELLI, D. 2014. Perturbation of m6A writers reveals two distinct classes of mRNA methylation at internal and 5′ sites. Cell Rep 8: 284–296.

SILVA, J., NICHOLS, J., THEUNISSEN, T. W., GUO, G., VAN OOSTEN, A. L., BARRANDON, O., WRAY, J., YAMANAKA, S., CHAMBERS, I. & SMITH, A. 2009. Nanog is the gateway to the pluripotent ground state. *Cell,* 138**,** 722-737.

SONG, H., FENG, X., ZHANG, H., LUO, Y., HUANG, J., LIN, M., JIN, J., DING, X., WU, S. & HUANG, H. 2019. METTL3 and ALKBH5 oppositely regulate m6A modification of TFEB mRNA, which dictates the fate of hypoxia/reoxygenation-treated cardiomyocytes. *Autophagy,* 15**,** 1419-1437.

STADTFELD, M. & HOCHEDLINGER, K. 2010. Induced pluripotency: history, mechanisms, and applications. *Genes & development,* 24**,** 2239-2263.

TAKAHASHI, K., TANABE, K., OHNUKI, M., NARITA, M., ICHISAKA, T., TOMODA, K. & YAMANAKA, S. 2007. Induction of pluripotent stem cells from adult human fibroblasts by defined factors. *cell,* 131**,** 861-872.

TAKAHASHI, K. & YAMANAKA, S. 2006. Induction of pluripotent stem cells from mouse embryonic and adult fibroblast cultures by defined factors. *cell,* 126**,** 663-676.

TANG, C., KLUKOVICH, R., PENG, H., WANG, Z., YU, T., ZHANG, Y., ZHENG, H., KLUNGLAND, A. & YAN, W. 2018. ALKBH5-dependent m6A demethylation controls splicing and stability of long 3′-UTR mRNAs in male germ cells. *Proceedings of the National Academy of Sciences,* 115**,** E325-E333.

THEUNISSEN, T. W., VAN OOSTEN, A. L., CASTELO-BRANCO, G., HALL, J., SMITH, A. & SILVA, J. C. 2011. Nanog overcomes reprogramming barriers and induces pluripotency in minimal conditions. *Current Biology,* 21**,** 65-71.

UTIKAL, J., POLO, J. M., STADTFELD, M., MAHERALI, N., KULALERT, W., WALSH, R. M., KHALIL, A., RHEINWALD, J. G. & HOCHEDLINGER, K. 2009. Immortalization eliminates a roadblock during cellular reprogramming into iPS cells. *Nature,* 460**,** 1145-1148.

VELYCHKO, S., ADACHI, K., KIM, K.-P., HOU, Y., MACCARTHY, C. M., WU, G. & SCHÖLER, H. R. 2019. Excluding Oct4 from Yamanaka cocktail unleashes the developmental potential of iPSCs. *Cell Stem Cell,* 25**,** 737-753. e4.

WANG, J., WANG, J., GU, Q., MA, Y., YANG, Y., ZHU, J. & ZHANG, Q. A. 2020. The biological function of m6A demethylase ALKBH5 and its role in human disease. *Cancer Cell International,* 20**,** 1-7.

WANG, X., LU, Z., GOMEZ, A., HON, G. C., YUE, Y., HAN, D., FU, Y., PARISIEN, M., DAI, Q. & JIA, G. 2014. N 6-methyladenosine-dependent regulation of messenger RNA stability. *Nature,* 505**,** 117-120.

WANG, X. Q., LO, C. M., CHEN, L., NGAN, E. S., XU, A. & POON, R. Y. 2017. CDK1-PDK1-PI3K/Akt signaling pathway regulates embryonic and induced pluripotency. *Cell Death & Differentiation,* 24**,** 38-48.

ZACCARA, S. & JAFFREY, S. R. 2020. A unified model for the function of YTHDF proteins in regulating m6A-modified mRNA. *Cell,* 181**,** 1582-1595. e18.

ZHANG, C., FU, J. & ZHOU, Y. 2019. A review in research progress concerning m6A methylation and immunoregulation. *Frontiers in immunology,* 10**,** 922.

ZHANG, C., SAMANTA, D., LU, H., BULLEN, J. W., ZHANG, H., CHEN, I., HE, X. & SEMENZA, G. L. 2016. Hypoxia induces the breast cancer stem cell phenotype by HIF-dependent and ALKBH5-mediated m6A-demethylation of NANOG mRNA. *Proceedings of the National Academy of Sciences,* 113**,** E2047-E2056.

ZHANG, S., ZHAO, B. S., ZHOU, A., LIN, K., ZHENG, S., LU, Z., CHEN, Y., SULMAN, E. P., XIE, K. & BÖGLER, O. 2017. m6A demethylase ALKBH5 maintains tumorigenicity of glioblastoma stem-like cells by sustaining FOXM1 expression and cell proliferation program. *Cancer cell,* 31**,** 591-606. e6.

ZHENG, G., DAHL, J. A., NIU, Y., FEDORCSAK, P., HUANG, C.-M., LI, C. J., VÅGBØ, C. B., SHI, Y., WANG, W.-L. & SONG, S.-H. 2013. ALKBH5 is a mammalian RNA demethylase that impacts RNA metabolism and mouse fertility. *Molecular cell,* 49**,** 18-29.

Figures

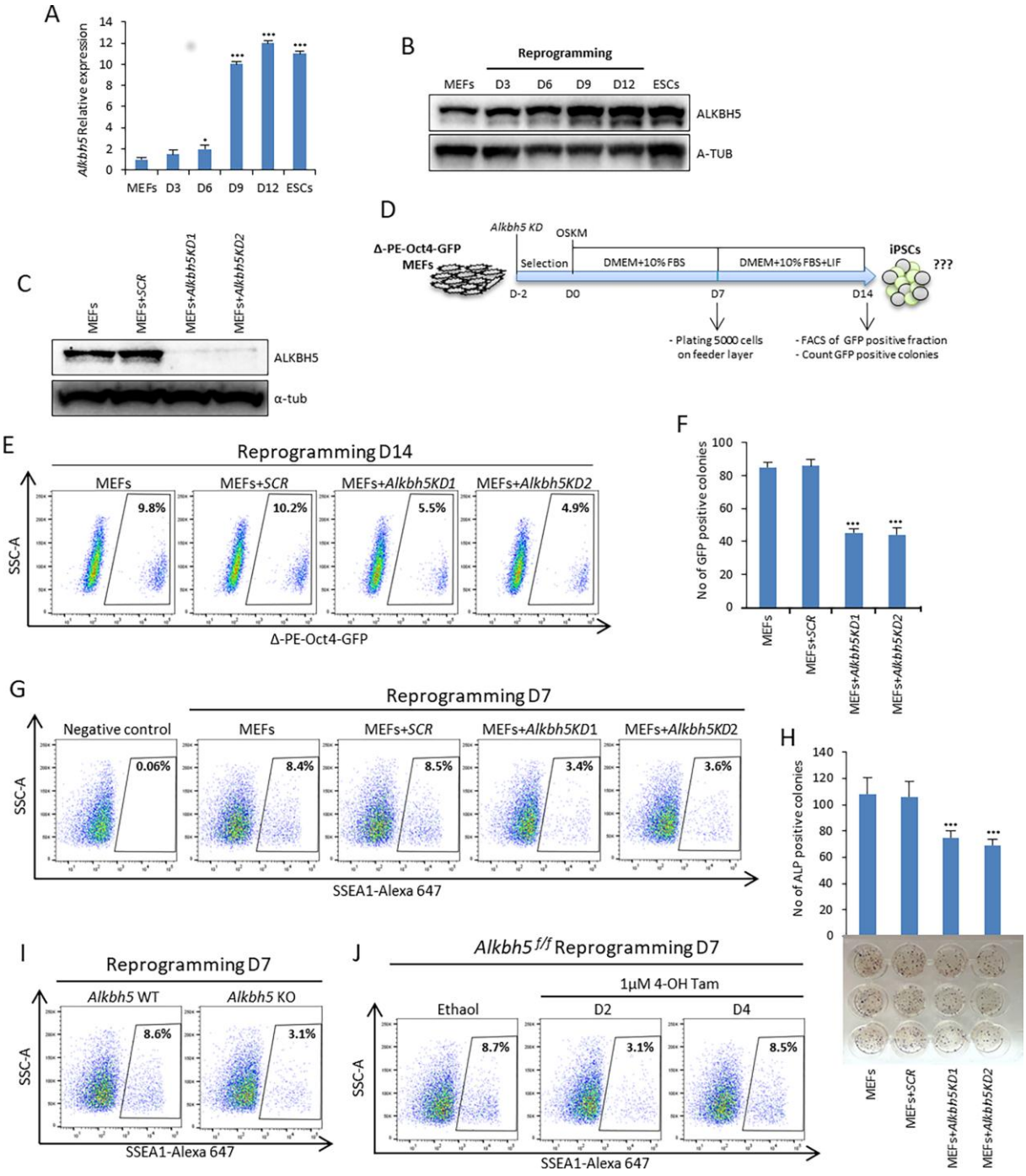

Figure 1. *Alkbh5* depletion impairs somatic cell reprogramming efficiency.

(A) Relative expression of *Alkbh5* during somatic cell reprogramming detected by qPCR. Mouse embryonic fibroblasts (MEFs) and mouse embryonic stem cells (ESCs) cultured in serum plus leukemia inhibitory factor LIF (S/L) were used as negative and positive controls

of pluripotency, respectively. Data are normalized to the housekeeping gene glyceraldehyde-3-phosphate dehydrogenase (*Gapdh*).

(B) Immunoblot analysis of ALKBH5 protein levels during reprogramming. Alpha-tubulin (A-TUB) was used as a loading control.

(C) Immunoblot analysis of ALKBH5 protein levels in MEFs after lentiviral infection with either scrambled or two different shRNAs targeting *Alkbh5*. *Scrambled* (*SCR*) shRNA used as a negative control. (A-TUB) was used as a loading control.

(D) Experimental design showing the timing of *Alkbh5* knockdown, onset of reprogramming, counting of GFP positive colonies, and FACS analysis of the Δ-PE-Oct4-GFP positive population.

(E) Fraction of Δ-PE-Oct4-GFP positive cells determined by FACS analysis after *Alkbh5* knockdown during the early phase of reprogramming.

(F) Number of Δ-PE-Oct4-GFP positive colonies on day 14 of reprogramming.

(G) Fraction of SSEA1 positive cells determined by FACS analysis after Alkbh5 knockdown during the early phase of reprogramming. Negative control is unreprogrammed MEFs.

(H) Reprogramming efficiency was measured by counting the number of ALP positive colonies.

(I) Fraction of SSEA1 positive cells determined by FACS for reprogrammed wild type (WT) and knockout (KO) *Alkbh5* MEFs assessed at day 7 of reprogramming.

(J) Fraction of SSEA1 positive cells determined by FACS analysis of reprogrammed homozygous floxed *Alkbh5* (*Alkbh5*$^{f/f}$) treated with ethanol as a control or 1 µM 4-hydroxytamoxifen (4-OH Tam) for depletion of *Alkbh5* at either day 2 or day 4. Data are shown as the mean ± SD; n = 3, *P < 0.05, **P < 0.01, and ***P < 0.001 mean ± SD deviation of triplicate samples.

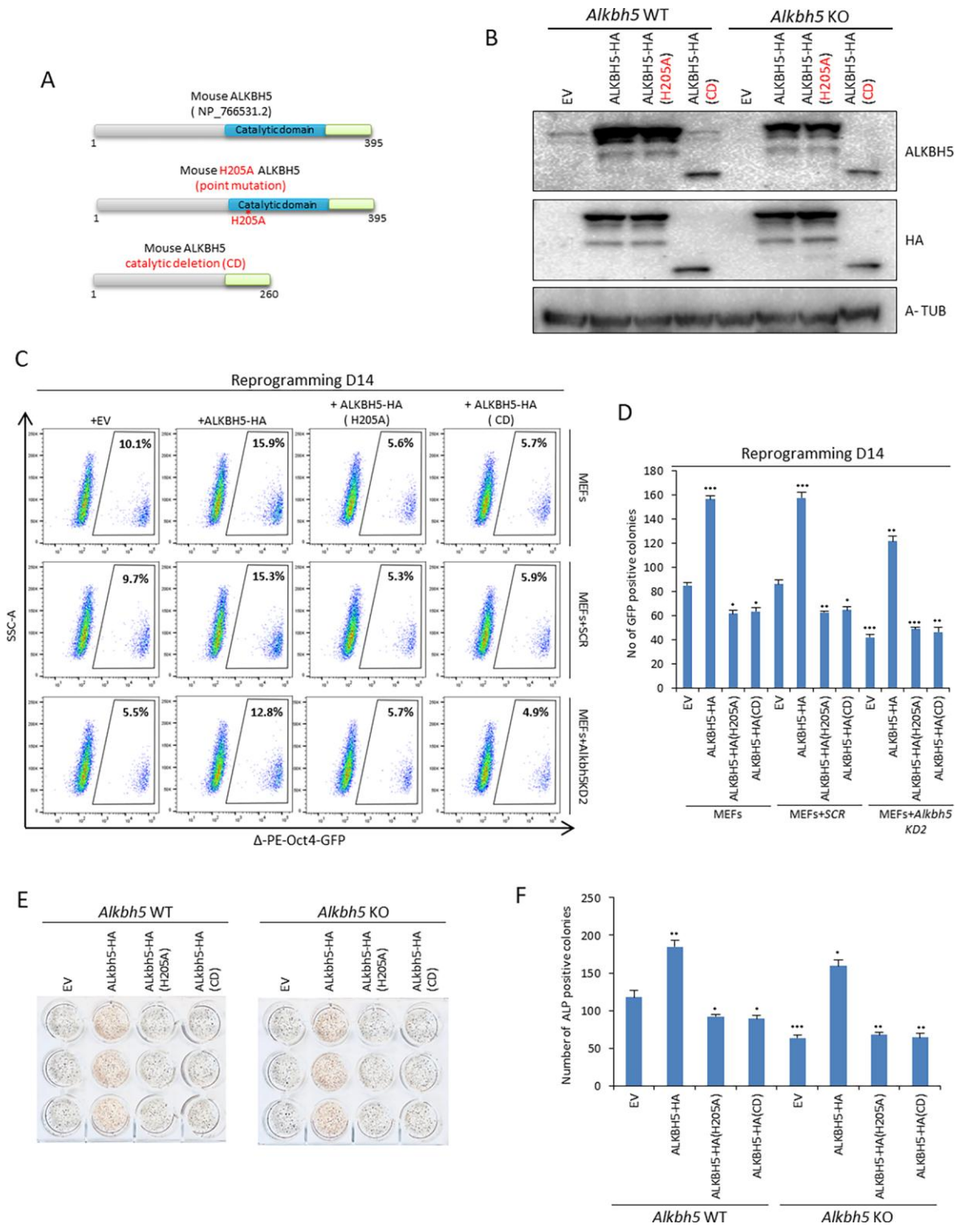

Figure 2. ALKBH5 regulates reprogramming through its catalytic activity.

(A) Schematic representation of mouse ALKBH5 protein. Upper panel represents the wild type (WT) ALKBH5. The middle panel represents catalytically inactive ALKBH5 with a point mutation in the catalytic domain, in which histidine (H) at position 205 is converted to alanine (A). The lower panel represents the catalytically deleted (CD) form of ALKBH5.

(B) Immunoblot analysis of ALKBH5 protein levels after overexpression of the HA-tagged forms of ALKBH5-HA, ALKBH5-HA (H205A), and ALKBH5-HA (CD) in either WT or KO *Alkbh5* MEFs on day 3 of reprogramming. Alpha-tubulin (A-TUB) was used as a loading control.

(C) Fraction of Δ-PE-Oct4-GFP positive cells determined by FACS analysis after overexpression of ALKBH5-HA, ALKBH5-HA (H205A), and ALKBH5-HA (CD) in uninfected MEFs or infection with either *SCR* shRNA or shRNA targeting the *Alkbh5* 3`UTR on day 14 of reprogramming.

(D) Number of Δ-PE-Oct4-GFP positive colonies on day 14 of reprogramming.

(E) Representative image of ALP staining on day 14.

(F) Reprogramming efficiency was measured by counting the number of ALP positive colonies presented in Figure 2E. Data are shown as the mean ± SD; $n = 3$, $*P < 0.05$, $**P < 0.01$, and $***P < 0.001$ mean ± SD deviation of triplicate samples.

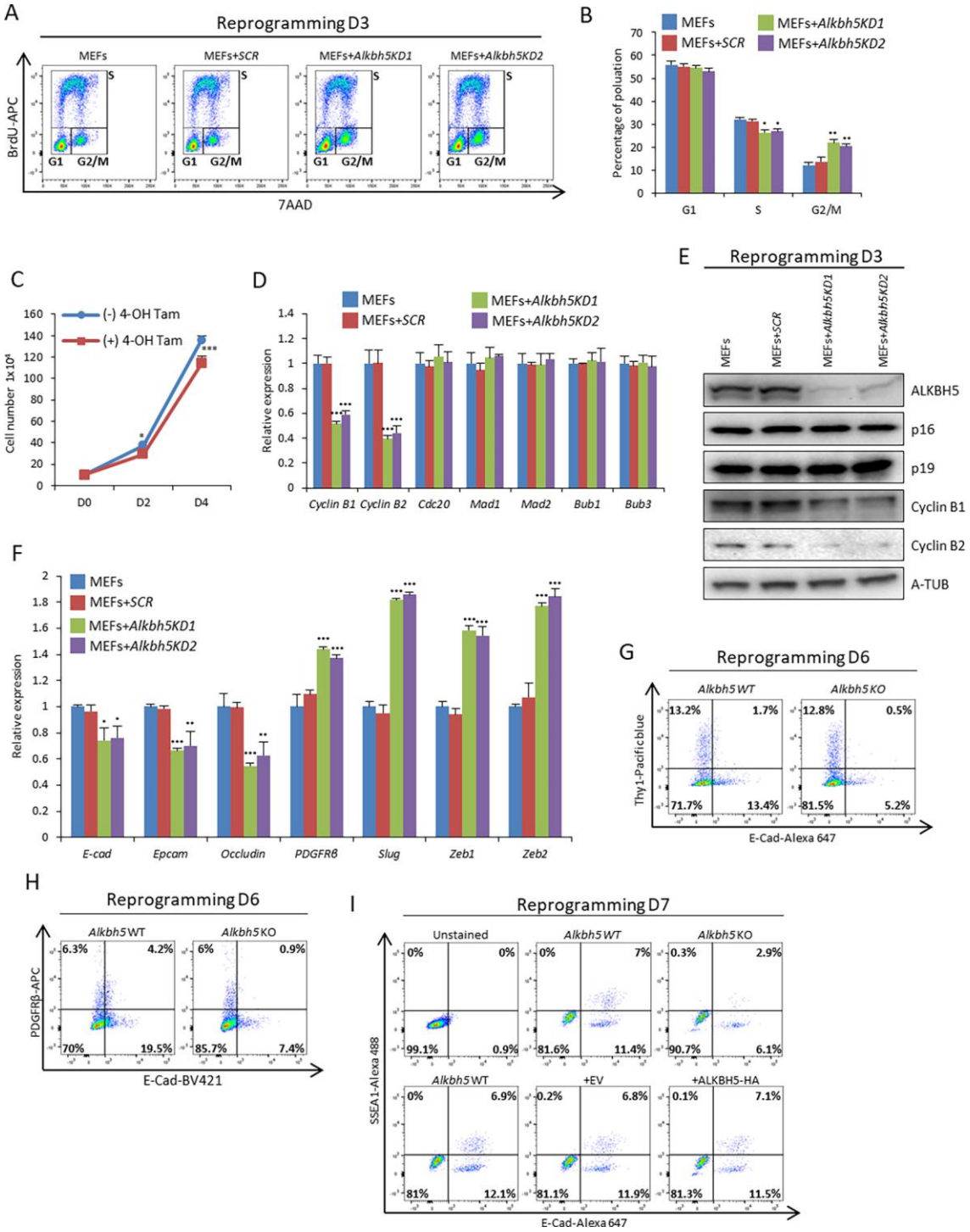

Figure 3. *Alkbh5* depletion induces G2/M cell cycle arrest and impairs the MET process.

(A) Cell proliferation was assessed by FACS measured by BrdU incorporation on day 3 of reprogramming using either scrambled shRNA or two different shRNAs targeting *Alkbh5*.

(B) Quantification of the mean percentage of each of the populations G1, S, and G2/M from FACS data shown in Figure 3A.

(C) Cell proliferation was assessed by counting *Alkbh5*$^{f/f}$ cells with or without the addition of 1 µM 4-OH Tam for *Alkbh5* depletion.

(D) Expression of mitotic checkpoint complex (MCC) factors as assessed by qPCR on day 3 of reprogramming using either scrambled shRNA or two different shRNAs targeting Alkbh5. The data were normalized to the housekeeping gene *Gapdh*.

(E) Immunoblot analysis of the protein levels of several cell cycle regulators on day 3 of reprogramming using either scrambled shRNA or two different shRNAs targeting *Alkbh5*. A-TUB was used as a loading control.

(F) Expression of mesenchymal and epithelial genes as assessed by qPCR on day 6 of reprogramming after infection either with scrambled shRNA or two different shRNAs targeting *Alkbh5*. The data were normalized to the housekeeping gene *Gapdh*.

(G) Estimation of E-cadherin (E-cad) and Thy-1 positive populations by FACS in WT and *Alkbh5* KO cells on day 6 of reprogramming.

(H) Estimation of E-cadherin (E-cad) and PDGFRβ positive populations by FACS in WT and KO *Alkbh5* MEFs on day 6 of reprogramming.

(I) Estimation of E-cadherin (E-cad) and SSEA1 positive populations by FACS in WT and *Alkbh5* KO MEFs or MEFs infected with either empty vector (EV) or ALKBH5-HA on day 7 of reprogramming. Data are shown as the mean ± SD; $n = 3$, $*P < 0.05$, $**P < 0.01$, and $***P < 0.001$ mean ± SD deviation of triplicate samples.

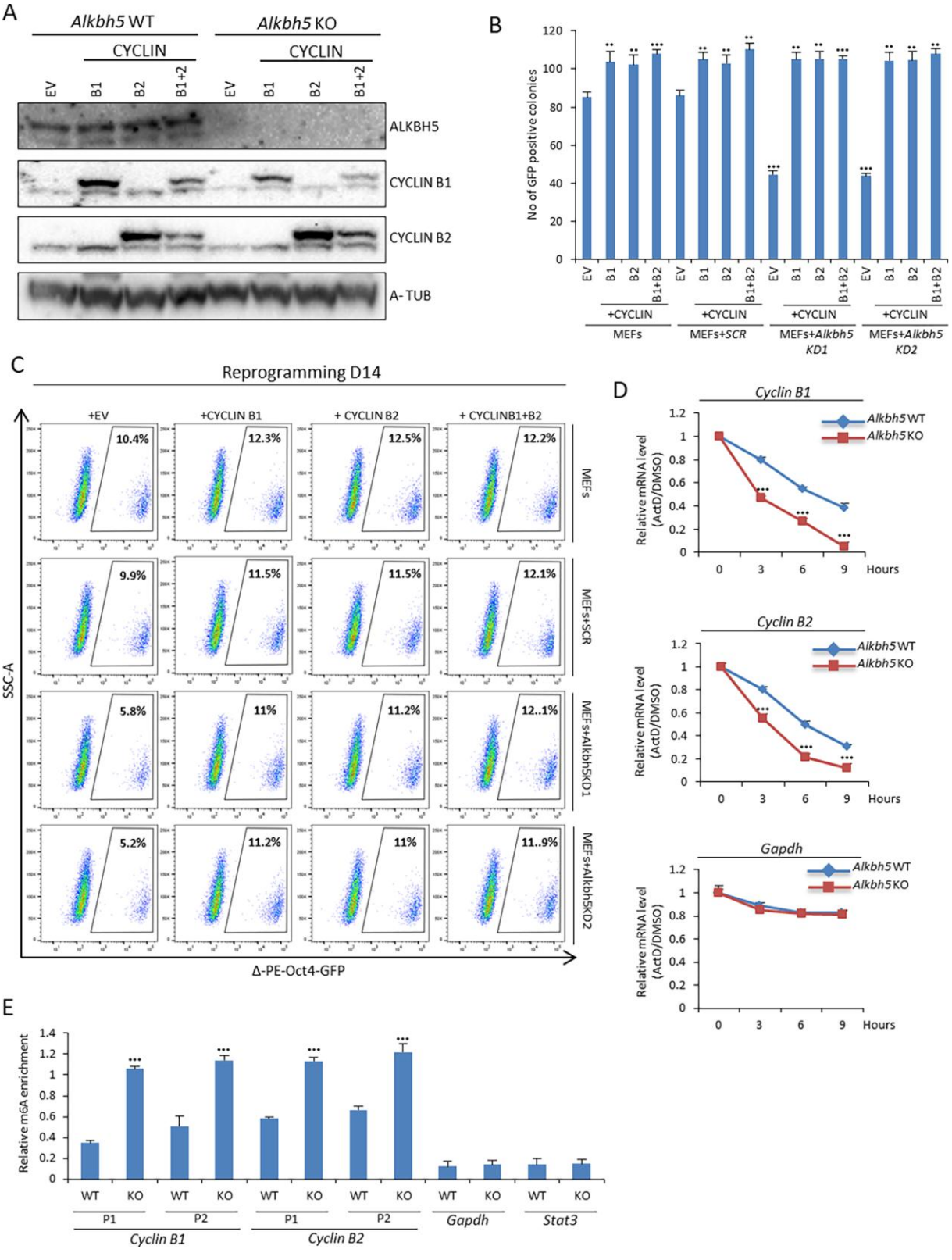

Figure 4. Overexpression of CYCLIN B1 and/or B2 enhances the reprogramming efficiency in WT and *Alkbh5* KO MEFs.

(A) Immunoblot analysis of CYCLIN B1 and B2 overexpression in WT and *Alkbh5* KO MEFs on day 3 of reprogramming. A-TUB was used as a loading control.

(B) Number of Δ-PE-Oct4-GFP positive colonies on day 14 of reprogramming.

(C) Fraction of Δ-PE-Oct4-GFP positive cells at day 14 of reprogramming determined by FACS analysis after overexpression of CYCLIN B1 and/or B2 in uninfected MEFs or infection with either *SCR* shRNA or two different shRNAs targeting *Alkbh5*.

(D) Stability of *CyclinB1 and B2* mRNA on day 3 of reprogramming. Both WT and *Alkbh5* KO MEFs were treated with either DMSO or 5 μM actinomycin D (ActD) at different time points from 0 to 9 hours. *Gapdh* was used as a negative control, and the data from cells treated with (ActD) were normalized to DMSO treated cells.

(E) m^6A-IP qPCR data of *CyclinB1 and B2* mRNA on day 3 of reprogramming in WT and *Alkbh5* KO MEFs using two different primers sets P1 and P2. Both primers were designed spanning m^6A rich region of *CyclinB1 and B2* transcripts. *Gapdh* and *Stat3* were used as negative controls. Data are shown as the mean ± SD; $n = 3$, $*P < 0.05$, $**P < 0.01$, and $***P < 0.001$.

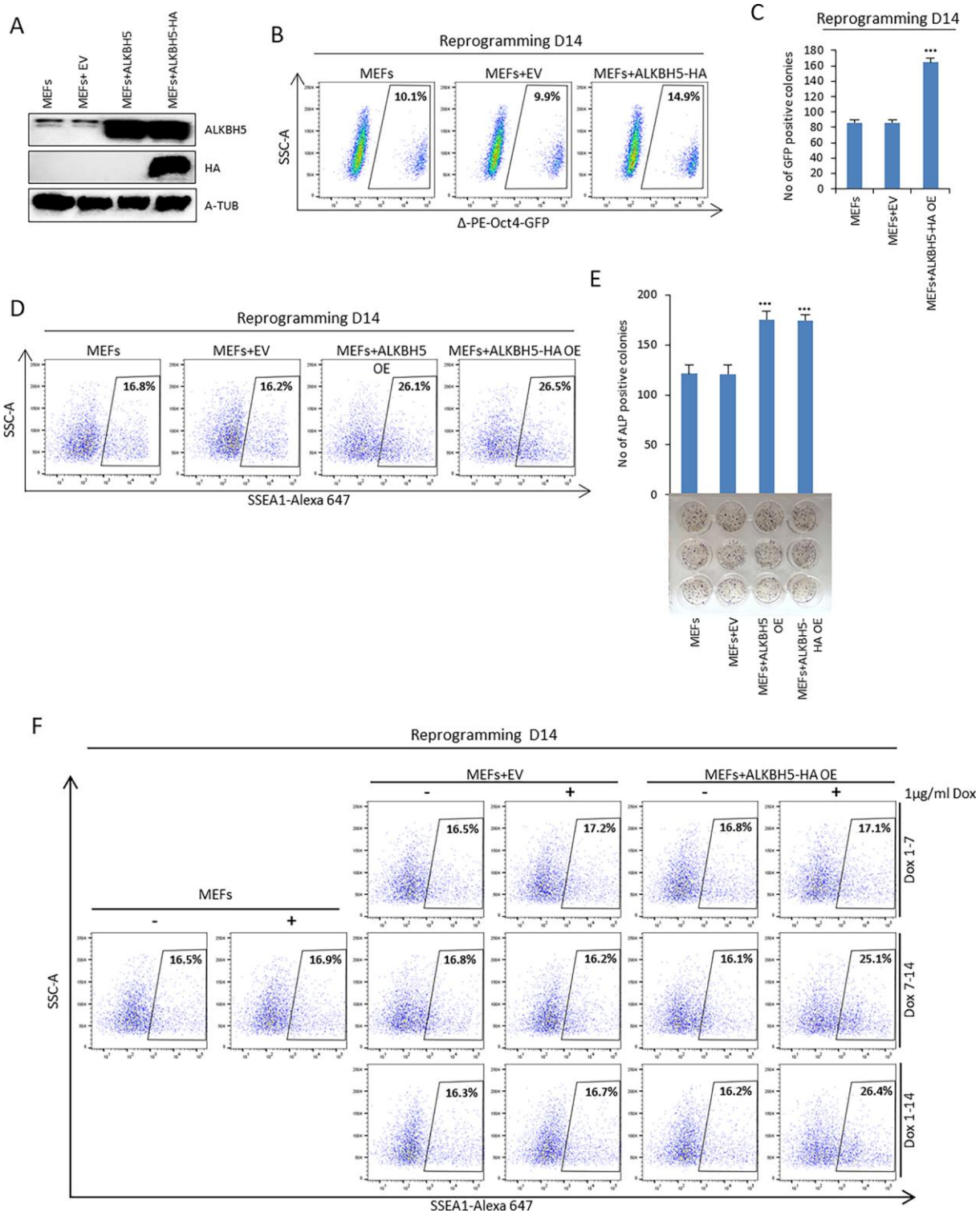

Figure 5. ALKBH5 overexpression enhances reprogramming efficiency.

(A) Immunoblot analysis of ALKBH5 protein levels after lentiviral infection of MEFs with empty vector, ALKBH5 or ALKBH5 tagged with HA (ALKBH5-HA). A-TUB was used as a loading control.

(B) Fraction of Δ-PE-Oct4-GFP positive cells at day 14 of reprogramming of MEFs, MEFs with empty vector (EV) and MEFs overexpressing ALKBH5-HA determined by FACS analysis.

(C) Number of Δ-PE-Oct4-GFP positive colonies on day 14 of reprogramming.

(D) Fraction of SSEA1 positive cells at day 14 of reprogramming of MEFs, MEFs with empty vector (EV) and MEFs overexpressing ALKBH5 or ALKBH5-HA determined by FACS.

(E) Reprogramming efficiency in MEFs overexpressing ALKBH5 or ALKBH5-HA was assessed by counting the number of ALP positive colonies on day 14 of reprogramming.

(F) Fraction of SSEA1 positive cells determined by FACS analysis on day 14 of reprogramming. Temporal overexpression of ALKBH5-HA by 1 μg/ml doxycycline (Dox) was carried out from day 1 to day 7, day 7 to day 14 or day 1 to day 14. MEFs were used as a negative control. Data are shown as the mean ± SD; $n = 3$, $*P < 0.05$, $**P < 0.01$, and $***P < 0.001$.

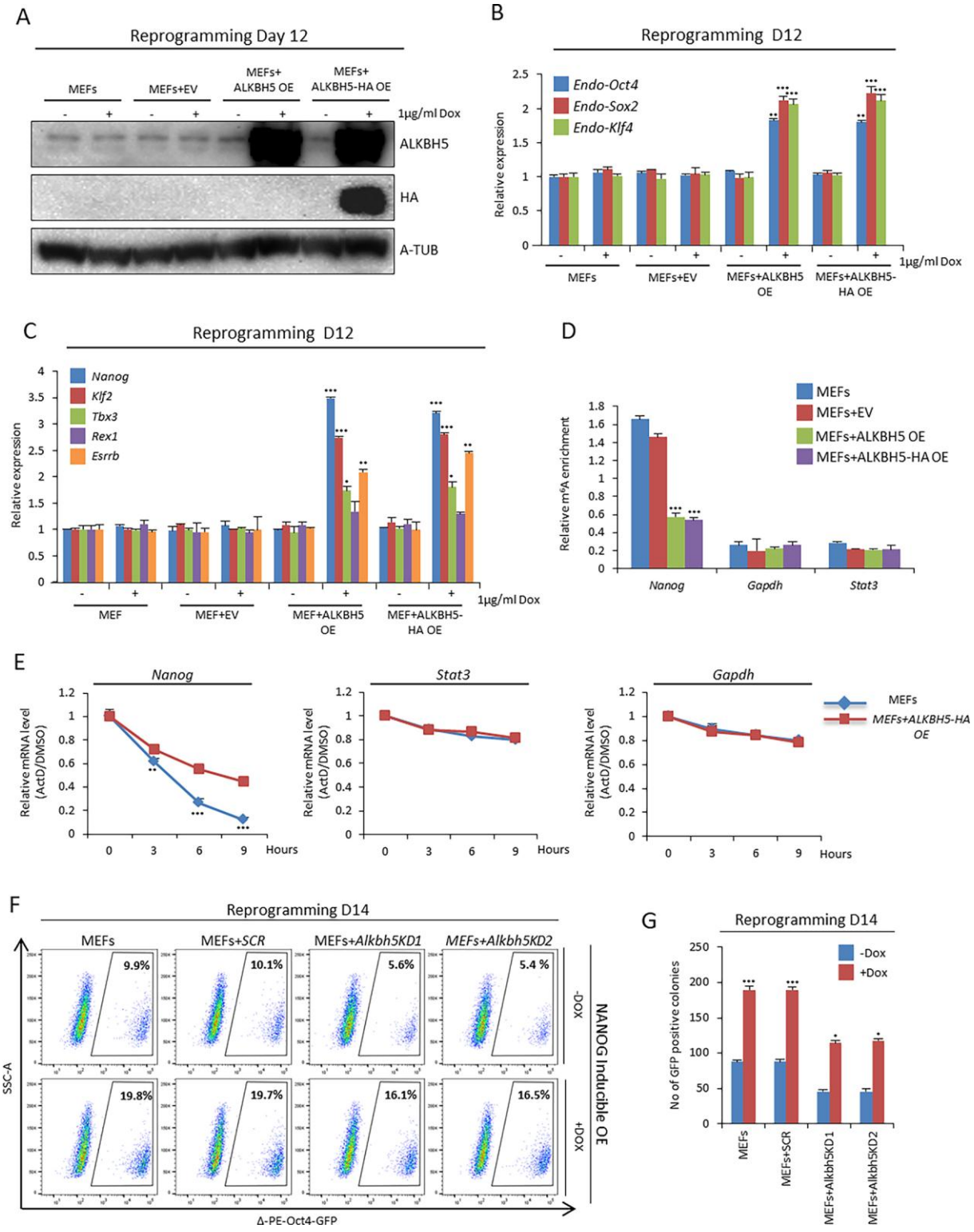

Figure 6. ALKBH5 overexpression in the late phase of reprogramming stabilizes *Nanog* transcripts, resulting in increased *Nanog* expression.

(A) Immunoblot analysis of ALKBH5 protein levels on day 12 of reprogramming. MEFs and Lentiviral infected MEFs with empty vector, ALKBH5 or ALKBH5-HA were treated with or

without Dox (1 µg/ml) on day 10 and cells were harvested on day 12. A-TUB was used as a loading control.

(B) Endogenous expression of pluripotency factors (*Oct4, Sox2,* and *Klf4*) in reprogrammed MEFs on day 12. MEFs and Lentiviral infected MEFs with empty vector, ALKBH5 or ALKBH5-HA were treated with or without Dox (1 µg/ml) on day 10 and cells were harvested on day 12 and analyzed by qPCR. The data were normalized to the housekeeping gene *Gapdh.*

(C) Expression of pluripotency markers in reprogrammed MEFs on day 12. MEFs and Lentiviral infected MEFs with empty vector, ALKBH5 or ALKBH5-HA were treated with or without Dox (1 µg/ml) on day 10 and cells were harvested on day 12 and analyzed by qPCR. The data were normalized to the housekeeping gene *Gapdh*.

(D) m^6A-IP qPCR data of *Nanog, Gapdh and Stat3* from reprogrammed MEFs on day 12. MEFs were infected with empty vector (EV) and MEFs overexpressing ALKBH5 or ALKBH5-HA on day 12 of reprogramming. m^6A qPCR data were normalized to the inputs.

(E) Stability of *Nanog* transcripts in reprogrammed MEFs as a control or MEFs with ALKBH5-HA overexpression on day 12 of reprogramming. Actinomycin D (ActD) was added on day 12. Cells were treated with either DMSO or 5 µM actinomycin D (ActD) at different time points from 0 to 9 hours. *Gapdh* and *Stat3* were used as negative controls, and the data of cells treated with 5 µM (ActD) were normalized to DMSO treated cells.

(F) Fraction of Δ-PE-Oct4-GFP positive cells on day 14 of reprogramming determined by FACS analysis using Dox-inducible overexpression of NANOG. Either WT MEFs or lentiviral infected MEFs with scrambled shRNA (SCR), or two different shRNAs targeting *Alkbh5*. Reprogrammed cells were treated with or without Dox (1 µg/ml) from day 8

(G) Number of Δ-PE-Oct4-GFP positive colonies on day 14 of reprogramming. Data are shown as the mean ± SD; n = 3, *P < 0.05, **P < 0.01, and ***P < 0.001.

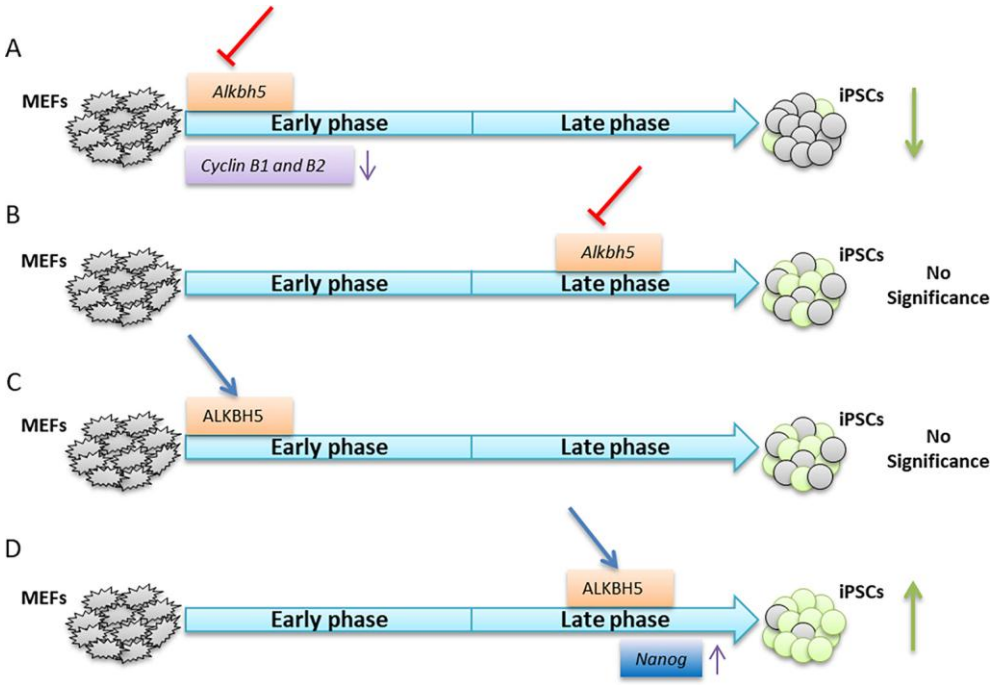

Figure 7. Model showing the biphasic role of ALKBH5 in somatic cell reprogramming.

(A) Depletion of *Alkbh5* specifically in the early phase of reprogramming decreases the reprogramming efficiency by reducing the expression of cyclin B1 and B2. (**B)** Depletion of *Alkbh5* in the late phase of reprogramming has no impact on reprogramming efficiency. **(C)** Overexpression of ALKBH5 in the early phase of reprogramming does not affect the reprogramming efficiency. **(D)** Overexpression of ALKBH5 in the late phase enhances the reprogramming efficiency by increasing *Nanog* expression.

Supplementary Fig. 1

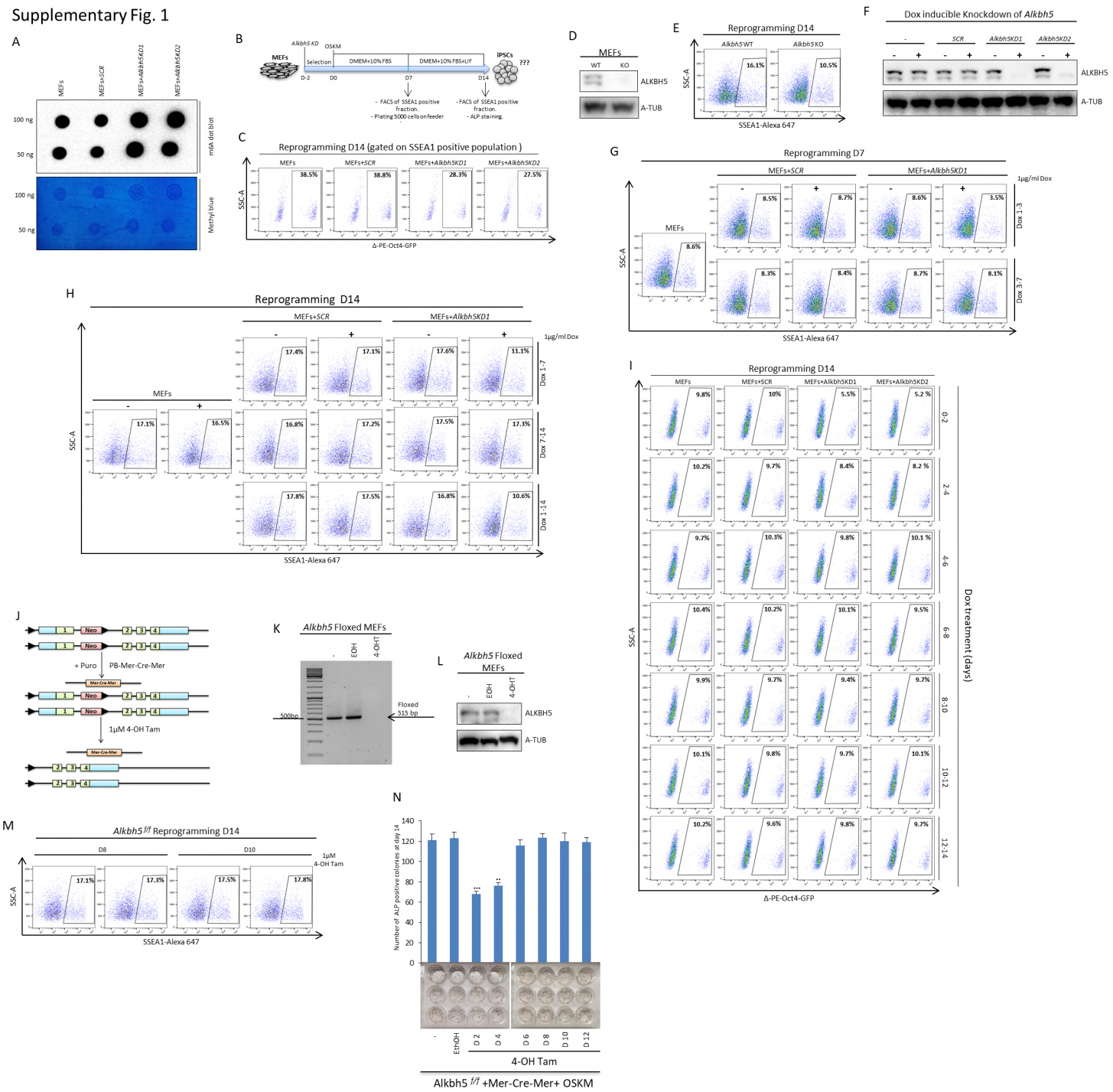

Fig.S1. Depletion of Alkbh5 in the efficiency. early stage impairs reprogramming

(A) m A dot blot [6]analysis of uninfected MEFs or MEFs infected either with lentiviral encoding scrambled shRNA (SCR) or two different shRNAs targeting Alkbh5 (upper panel). Methyl blue staining was used as a control to eliminate the difference in loaded mRNA amount (lower panel).

(B) Experimental design showing the timing of Alkbh5 knockdown, onset of reprogramming, and SSEA1 and ALP detection.

(C) Fraction of Δ-PE-Oct4-GFP-positive cells gated on the SSEA1-positive fraction determined by FACS analysis on day 14 of reprogramming.

(D) Immunoblot analysis of ALKBH5 protein levels in WT and Alkbh5 KO MEFs. A-TUB was used as loading control.

(E) Fraction of SSEA1-positive cells determined by FACS in WT and Alkbh5 KO reprogrammed MEFs on day 14 of reprogramming.

(F) Immunoblot analysis of ALKBH5 protein levels in MEFs infected with lentivirus encoding scrambled shRNA and two different shRNAs targeting Alkbh5. After selection with puromycin for 2 days, cells were treated with 1 μg/ml Dox to induce the expression of shRNA. A-TUB was used as a loading control.

(G) Fraction of SSEA1-positive cells determined by FACS in reprogrammed MEFs infected either with scrambled shRNA or shRNA targeting Alkbh5 with or without 1 μg/ml Dox treatment on day 7 of reprogramming. MEFs were used as a negative control.

(H) Fraction of SSEA1-positive cells determined by FACS in reprogrammed MEFs infected either with scrambled shRNA or shRNA targeting Alkbh5 with or without 1 μg/ml Dox treatment on day 14 of reprogramming. MEFs were used as a negative control.

(I) Fraction of the Δ-PE-Oct4-GFP-positive population was determined by FACS on day 14 of reprogramming throughout the whole reprogramming process. MEFs were infected either with scrambled shRNA or shRNA targeting Alkbh5 and treated with 1 μg/ml Dox every two days.

(J) Experimental design for Alkbh5 depletion. Homozygous Alkbh5$^{f/f}$ MEFs were derived from mice at 13.5 days post-coitum (d.p.c) before transfection with PB-GAG-Mer-Cre-Mer, selection with puromycin for 2 days, and treatment with 1 μM 4-OH Tam for induction of Cre to remove Alkbh5.

(K) Genotyping of homozygous Alkbh5$^{f/f}$ MEFs untreated or treated with either ethanol (negative control) or 1 μM 4-OH Tam for Alkbh5 removal. The band corresponds to the neomycin (Neo) PCR amplicon of 515 base pairs (bps).

(L) ALKBH5 immunoblot analysis of homozygous Alkbh5$^{f/f}$ MEFs untreated or treated with either ethanol (negative control) or 1 μM 4-OH Tam for Alkbh5 removal.

(M) Fraction of SSEA1-positive cells determined by FACS in reprogrammed MEFs on day 14 of reprogramming. Reprogrammed homozygous Alkbh5$^{f/f}$ MEFs treated with 1 μM 4-OH Tam for Alkbh5 depletion at day 8 or day 10 of reprogramming.

(N) Reprogramming efficiency as assessed by counting the number of ALP-positive colonies on day 14 of reprogramming. Reprogrammed homozygous Alkbh5$^{f/f}$ MEFs treated with 1 μM 4-OH Tam for Alkbh5 at days 2, 4, 6, 8, 10 and 12 of reprogramming, and ethanol treatment was used as a negative control. Data are shown as the mean ± SD; $n = 3$, $^{*}P < 0.05$, $^{**}P < 0.01$, and $^{***}P < 0.001$.

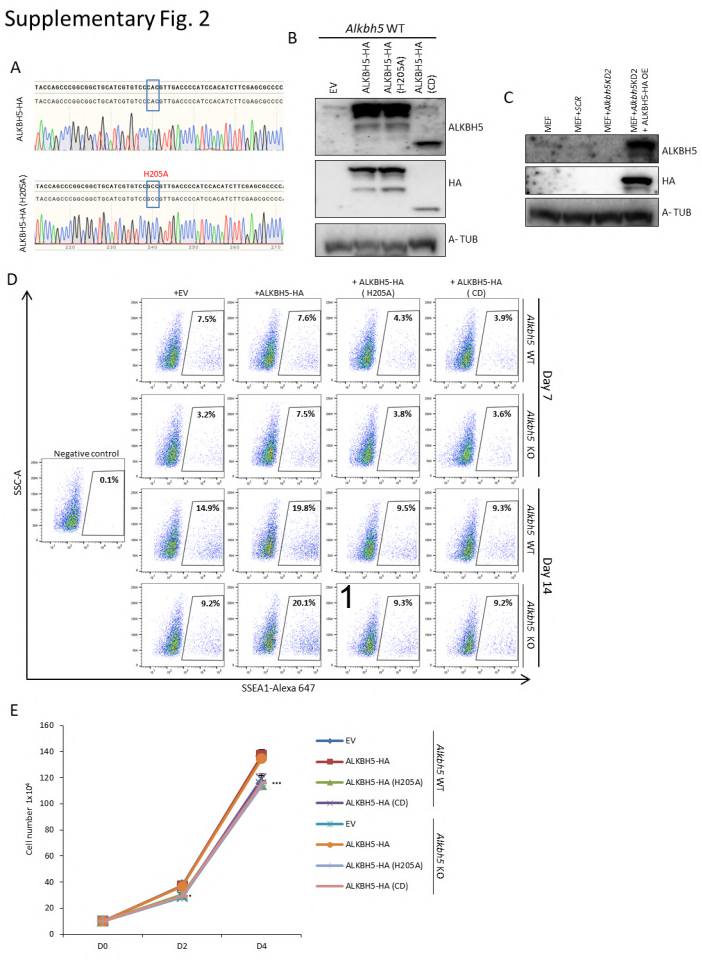

Fig. S2. ALKBH5 regulates somatic reprogramming through catalytic activity.

(A) Sequencing chromatogram of WT ALKBH5-HA and point mutated ALKBH5 (H205A); the blue box indicates the modified histidine to alanine amino acid.

(B) Immunoblot analysis of ALKBH5 in MEFs infected with empty vector (EV), ALKBH5-HA, ALKBH5-HA (H205A), or ALKBH5-HA (CD). A-TUB was used as a loading control.

(C) Immunoblot analysis of ALKBH5 in MEFs infected with either *SCR* shRNA, shRNA targeting the 3ÙTR of *Alkbh5* or shRNA targeting the 3ÙTR of *Alkbh5* and ALKBH5-HA. A-TUB was used as a loading control.

(D) Fraction of SSEA1-positive cells determined by FACS in reprogrammed MEFs on days 7 and 14 of reprogramming. Both WT and KO *Alkbh5* MEFs were infected with empty vector (EV), ALKBH5-HA, ALKBH5-HA (H205A), or ALKBH5-HA (CD). Unstained MEFs used as a negative control.

(E) Cell proliferation assay on day 4 of reprogramming. Both WT and KO *Alkbh5* MEFs were infected with empty vector (EV), ALKBH5-HA, ALKBH5-HA (H205A), or ALKBH5-HA (CD). Data are shown as the mean ± SD; n = 3, *P < 0.05, **P < 0.01, and ***P < 0.001.

Supplementary Fig. 3

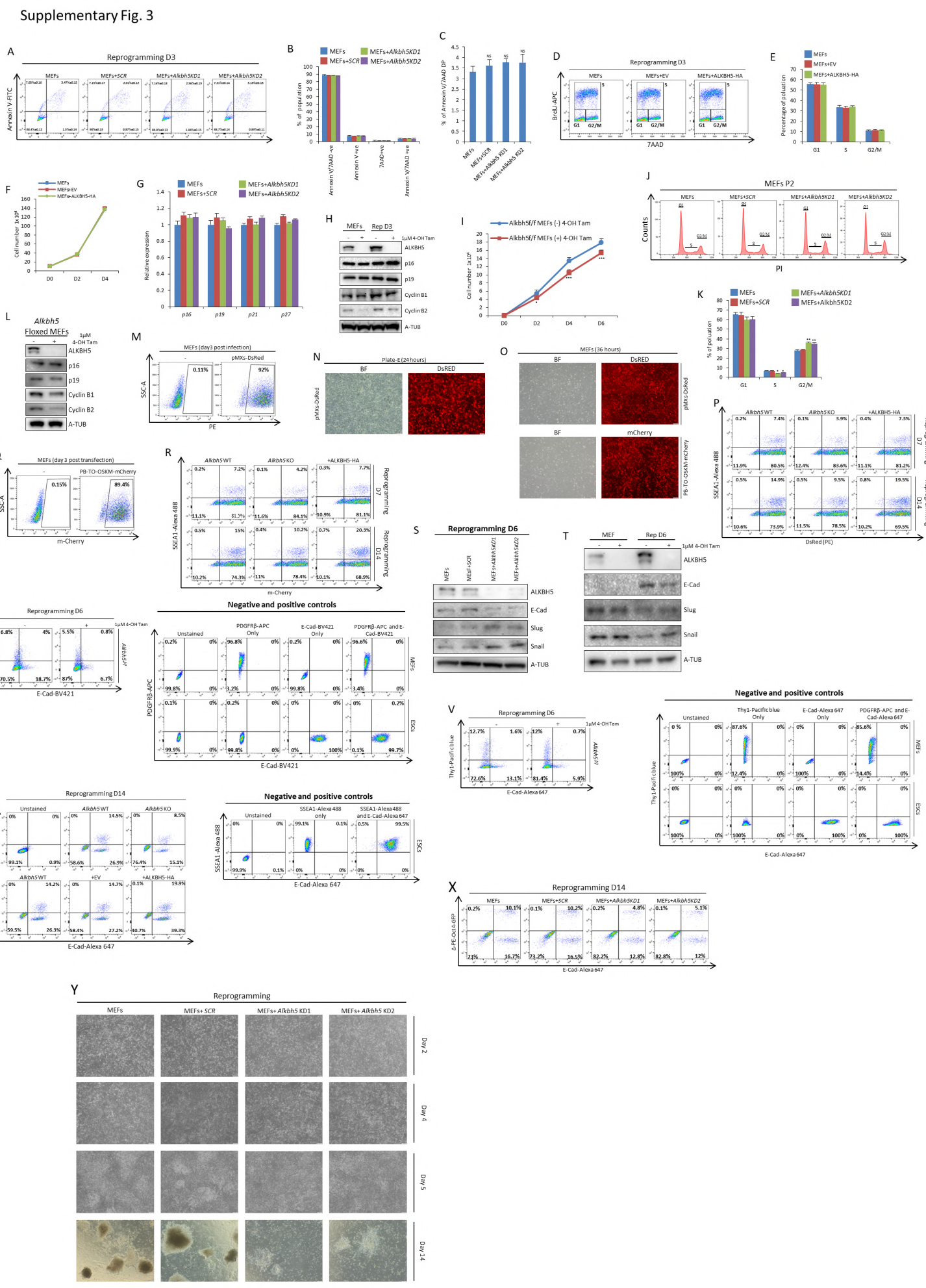

Fig. S3. *Alkbh5* removal impairs cell reprogrammed proliferation in either MEFs or MEFs without increasing apoptosis.

(A) Fraction of apoptotic cells determined by FACS in reprogrammed MEFs uninfected or infected either by scrambled shRNA or two shRNAs targeting *Alkbh5* was assessed at day 3 of reprogramming using double staining with Annexin V and 7AAD staining.

(B) Analysis of cell apoptosis data determined by FACS in (Supplementary Fig. 3 A), each of 7AAD or Annexin V single positive (+ve) or negative (-ve), Annexin V/7AAD +ve or Annexin V/7AAD –ve.

(C) Only the Annexin V/7AAD double-positive population from Supplementary Fig. 2 B was used to clarify the insignificance among reprogrammed MEFs uninfected or infected either by scrambled shRNA or two shRNAs targeting *Alkbh5*.N. S; Not significant.

(D) Cell proliferation was assessed by FACS measured by BrdU incorporation on day 3 of reprogramming using uninfected MEFs or infected MEFs with either EV or ALKBH5-HA.

(E) Quantification of the mean percentage of each of the populations G1, S and G2/M from FACS data shown in supplementary Fig. 3D. The mean percentage of each population was written as the mean ± S.D.

(F) Cell proliferation assay on day 4 of reprogramming using uninfected MEFs or infected MEFs with either EV or ALKBH5-HA.

(G) Expression of G1 cell cycle regulators as assessed by qPCR at day 3 of reprogramming in reprogrammed MEFs uninfected or infected either by scrambled shRNA or two shRNAs targeting *Alkbh5* was estimated at day 3 of reprogramming. The data were normalized to the housekeeping gene *Gapdh*.

(H) Immunoblot analysis of the protein levels of several cell cycle regulators in either homozygous *Alkbh5*$^{f/f}$ MEFs or reprogrammed homozygous *Alkbh5*$^{f/f}$ MEFs on day 3 with or without treatment with 1 µM 4-OH Tam to remove *Alkbh5*. A-TUB was used as a loading control.

(I) Cell proliferation assay of homozygous *Alkbh5*^{ff} MEFs with or without treatment with 1 µM 4-OH Tam to remove *Alkbh5* at different time points.

(J) Cell cycle analysis detected by PI staining and analyzed by FACS in uninfected MEFs or infected with scrambled shRNA or two different shRNAs targeting *Alkbh5*.

(K) Quantification of G1, S, and G2/M cell cycle phase data (Supplementary Fig. 3J).

(L) Immunoblot analysis of the protein levels of several cell cycle regulators in homozygous *Alkbh5*$^{f/f}$ MEFs with or without treatment with 1 µM 4-OH Tam to remove Alkbh5. A-TUB used as a loading control.

(M) (M) FACS analysis of retroviral infection efficiency in MEFs using pMXs-DsRed after 3 days.

(N) (N) Bright-field and fluorescent images of Plate-E transfected with pMXs-DsRed vector. Scale bar 200µm.

(O) (O) Bright-field and fluorescent images of MEFs infected with either retroviral pMXs-DsRed or piggyback-TO-OSKM-mCherry treated with Dox. Scale bar 200µm.

(P) FACS analysis of SSEA1- and DsRed-positive populations of reprogrammed MEFs on days 7 and 14 of reprogramming using WT and KO Alkbh5 MEFs or MEFs infected with ALKBH5-HA.

(Q) FACS analysis of transfection efficiency in MEFs using piggyback-TO-OSKM-mCherry treated with Dox after 3 days.

(R) FACS analysis of SSEA1- and mCherry-positive populations of reprogrammed MEFs on days 7 and 14 of reprogramming using WT and KO Alkbh5 MEFs or MEFs infected with ALKBH5-HA.

(S) Immunoblot analysis of the protein levels of mesenchymal and epithelial markers on day 6 of reprogramming after infection with either scrambled shRNA or two different shRNAs targeting *Alkbh5*. A-TUB was used as a loading control.

(T) Left panel shows FACS analysis of E-Cad- and PDGFRβ-positive populations using *Alkbh5*$^{f/f}$ MEFs with or without 1 µM 4-OH-Tam on day 6 of reprogramming. Right panel shows the optimization of gating. MEFs and ESCs were used as negative and positive markers for MET transition, respectively.

(U) The left panel shows FACS analysis of E-Cad- and Thy1-positive populations using *Alkbh5*$^{f/f}$ MEFs with or without 1 µM 4-OH-Tam on day 6 of reprogramming. Right panel shows the optimization of gating. MEFs and ESCs were used as negative and positive markers for MET transition, respectively.

(V) The left panel shows FACS analysis of E-Cad- and SSEA1-positive populations on day 14 of reprogramming. Right panel shows the optimization of gating. ESCs were used as a positive control.

(W) FACS analysis of Δ-PE-Oct4-GFP- and E-Cad-positive populations on day 14 of reprogramming using uninfected MEFs or infected with either *SCR* or two shRNAs targeting *Alkbh5*.

(X) Immunoblot analysis of the protein levels of both mesenchymal and epithelial markers in either homozygous *Alkbh5*$^{f/f}$ MEFs or reprogrammed homozygous *Alkbh5*$^{f/f}$ MEFs on day 6 with or without treatment with 1 µM 4-OH Tam to remove *Alkbh5*. A-TUB used as a loading control.

(Y) Phase contrast images of tracking morphological changes during reprogramming. Reprogrammed MEFs uninfected or infected either by scrambled shRNA or two shRNAs targeting *Alkbh5* were estimated at days 2, 4, 6 and 14 of reprogramming. Scale bar 200µm. Data are shown as the mean ± SD; n = 3, *P < 0.05, **P < 0.01, and ***P < 0.001.

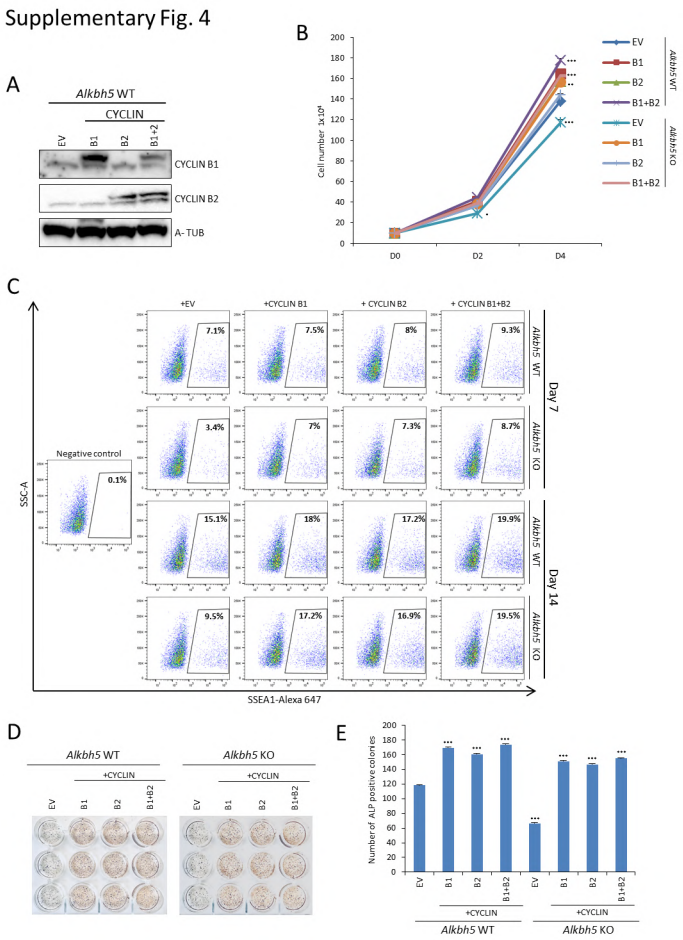

Fig. S4. CYCLIN B1 and/or B2 proliferation overexpression enhances both cell and reprogramming.

(A) Immunoblot of CYCLIN B1 and B2 in WT *Alkbh5*MEFs infected with either empty vector (EV), CYCLIN B1, B2, or both together. A-TUB used as a loading control.

(B) Cell proliferation assay on day 4 of reprogramming. Both WT and KO *Alkbh5* MEFs were infected with empty vector (EV), CYCLIN B1, B2, or both.

(C) Fraction of SSEA1-positive cells determined by FACS in reprogrammed MEFs on days 7 and 14 of reprogramming. Both WT and KO *Alkbh5* MEFs were infected with empty vector (EV), CYCLIN B1, B2, or both. Unstained MEFs used as a negative control.

(D) Representative image of ALP staining on day 14.

(F) Reprogramming efficiency was measured by counting the number of ALP-positive colonies represented in Supplementary Fig. 4D. Data are shown as the mean ± SD; $n = 3$, $^{*}P < 0.05$, $^{**}P < 0.01$, and $^{***}P < 0.001$ mean ± SD deviation of triplicate samples.

Supplementary Fig. 5

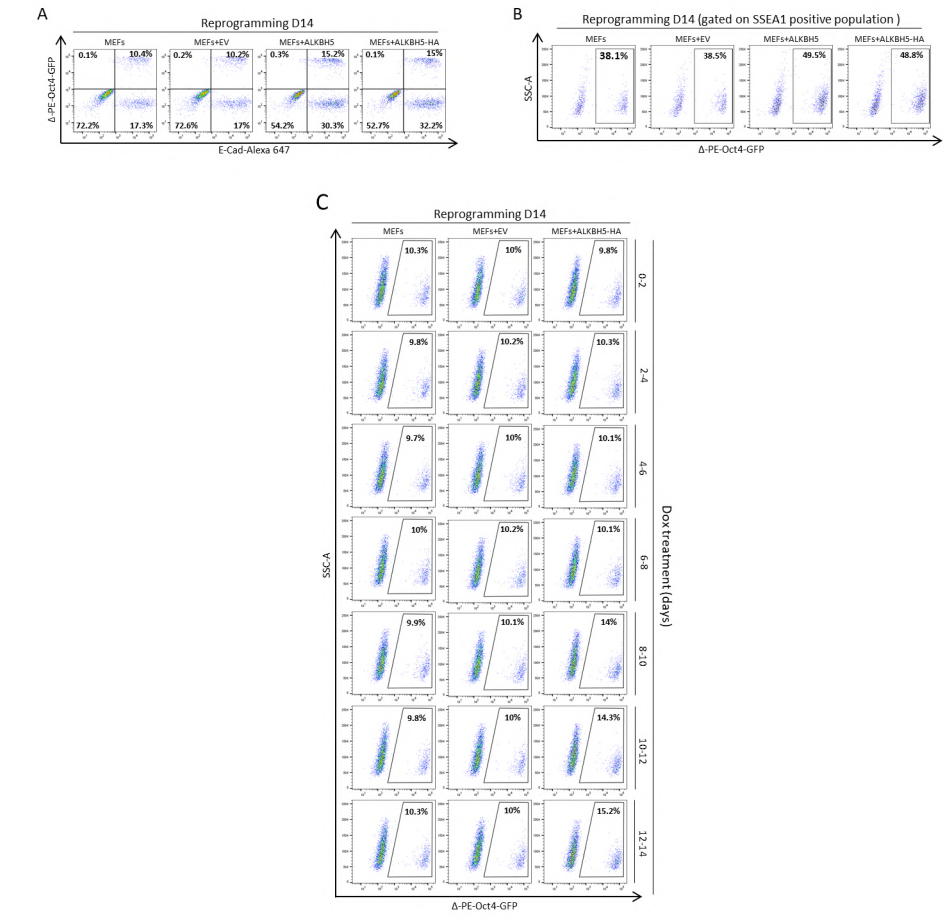

Fig. S5. ALKBH5 overexpression in the late phase enhances reprogramming efficiency.

(A) FACS analysis of Δ-PE-Oct4-GFP- and E-Cad-positive populations on day 14 of reprogramming using uninfected MEFs or infected with EV, ALKBH5-HA, and ALKBH5-HA.

(B) FACS analysis of the Δ-PE-Oct4-GFP-positive population gated on the SSEA1-positive fraction on day 14 of reprogramming.

(C) FACS analysis of the Δ-PE-Oct4-GFP-positive population throughout the whole reprogramming process. Uninfected MEFs and MEFs infected with EV or ALKBH5-HA were induced by Dox treatment every two days and analyzed on day 14.

Supplementary Fig. 6

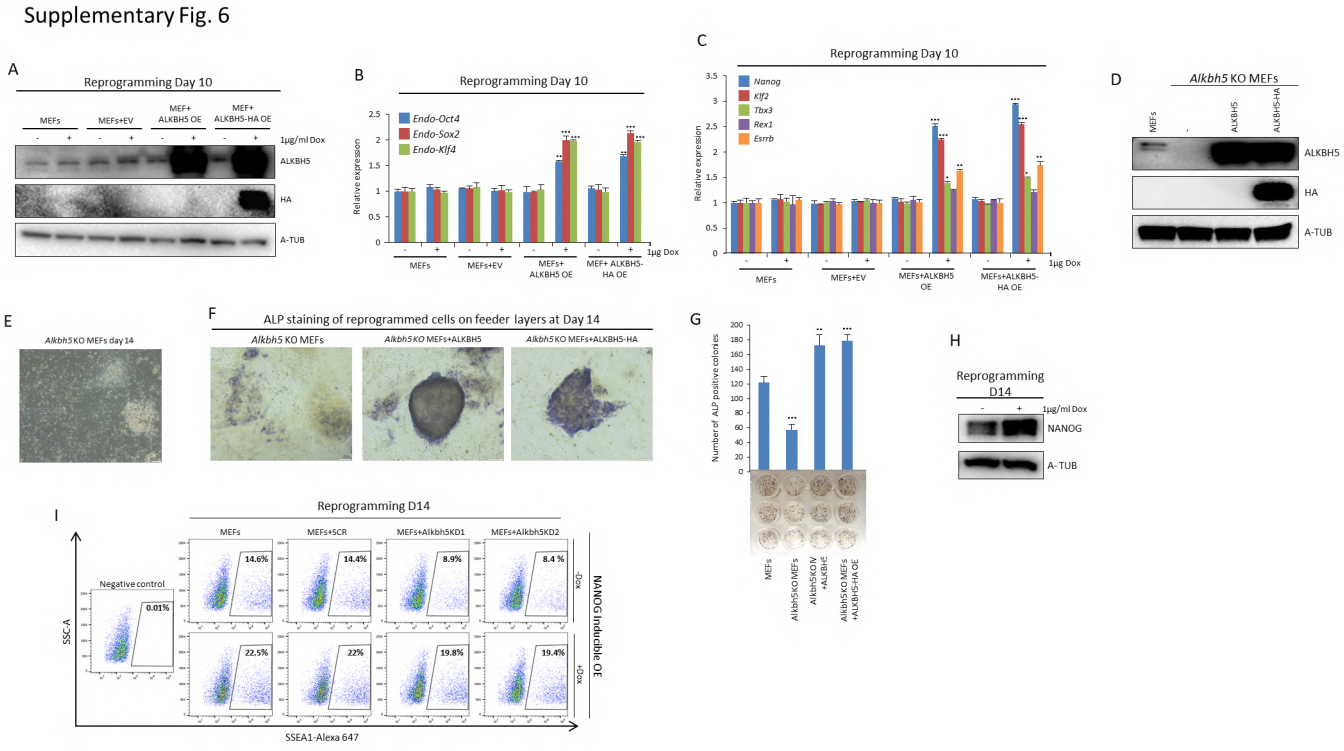

Fig. S6. ALKBH5 overexpression in the late phase of reprogramming enhances reprogramming efficiency by increasing *Nanog* expression.

(A) Immunoblot analysis of ALKBH5 protein levels after lentiviral infection of reprogrammed MEFs on day 12 with empty vector, ALKBH5 or ALKBH5-HA. Dox (1 µg/ml) was added on day 8, and the cells were harvested on day 10. A-TUB used as loading control.

(B) Endogenous expression of pluripotency factors (*Oct4, Sox2, Klf4*) as detected by qPCR on day 10 of reprogramming using either empty vector, ALKBH5 or ALKBH5-HA. The data were normalized to the housekeeping gene *Gapdh*.

(C) Expression of pluripotency markers detected by qPCR on day 12 of reprogramming using EV, ALKBH5 or ALKBH5-HA. The data were normalized to the housekeeping gene *Gapdh*.

(D) Immunoblot of ALKBH5 in WT and KO *Alkbh5* MEFs and rescued KO MEFs infected with lentiviral ALKBH5 and ALKBH5-HA. A-TUB used as a loading control.

(E) Phase contrast image of *Alkbh5* KO reprogrammed MEFs at day 14 of reprogramming. Scale bar 200µm.

(F) Phase contrast image of ALP-stained reprogrammed *Alkbh5* KO MEFs and rescued KO MEFs infected with either ALKBH5 or ALKBH5-HA at day 14. Scale bar 200µm.

(G) Reprogramming efficiency as assessed by counting the number of ALP-positive colonies on day 14 of reprogramming.

(H) Immunoblot of NANOG in MEFs infected with Dox-inducible NANOG with or without Dox treatment on day 14. A-TUB used as a loading control.

(I) Fraction of SSEA1-positive cells determined by FACS in reprogrammed MEFs on day 14 of reprogramming. NANOG was induced after 1 µg/ml Dox treatment. Data are shown as the mean ± SD; n = 3, *P < 0.05, **P < 0.01, and ***P < 0.001.

Supplementary Fig.7

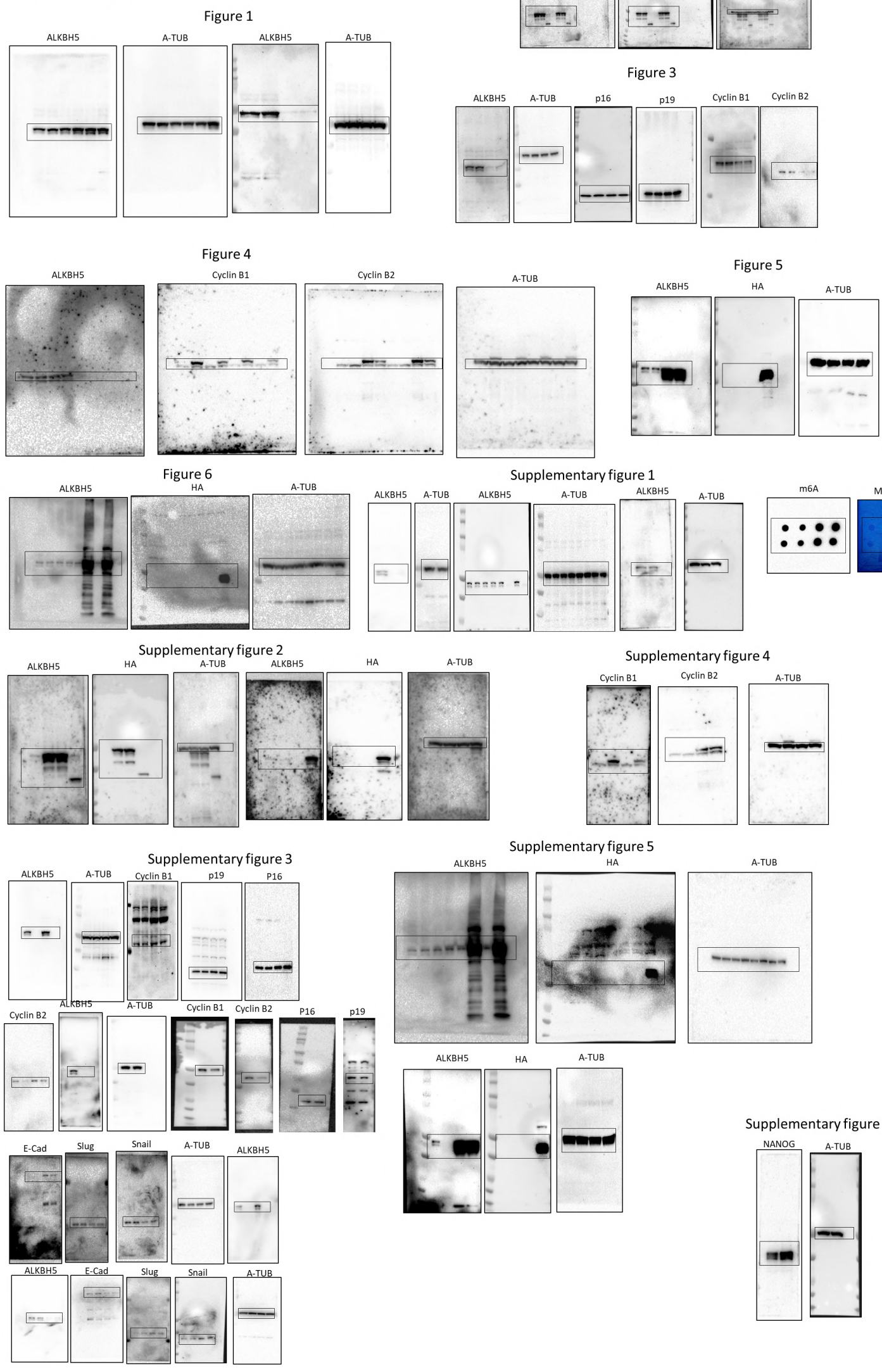

Fig. S7. Blot transparency for all western blot data including main and supplementary figures.

Table S1. List of primers for qPCR, cloning and m6A IP

Click here to download Table S1

Table S2. List of antibodies used

Click here to download Table S2